ADVANCED FUNCTIONAL MATERIALS
www.afm-journal.de

Self-Powered Tactile Sensor Array Systems Based on the Triboelectric Effect

Juan Tao, Rongrong Bao, Xiandi Wang, Yiyao Peng, Jing Li, Sheng Fu, Caofeng Pan,* and Zhong Lin Wang**

With the arrival of intelligent terminals, tactile sensors which are capable of sensing various external physical stimuli are considered among the most vital devices for the next generation of smart electronics. To create a self-powered tactile sensor system that can function sustainably and continuously without an external power source is of crucial significance. An overview of the development in self-powered tactile sensor array system based on the triboelectric effect is systematically presented. The combination of multi-functionalization and high performance of tactile sensors aimed at achieving highly comprehensive performance is presented. For the tactile sensor unit, a development is summarized based on the two primary modes which are vertical contact–separation and single-electrode. For the pressure mapping array, the resolution is significantly enhanced by the novel cross-type configuration based on the single-electrode mode. Integrated with other mechanisms, the performance will be further elevated by broadening of the detect range and realizing of visualization of pressure imaging. Then, two main applications of human–machine interaction (HMI) and trajectory monitoring are comprehensively summarized. Finally, the future perspectives of self-powered tactile sensor system based on triboelectric effect are discussed.

1. Introduction

Significant progress has been achieved in mobile networks and smart terminals in the past few decades, which has motivated the aspiring investigation of various intelligent sensors for the growing demand in our daily life. Particularly, flexible tactile sensors endowed with basic perceived capability of sensing external physical stimuli have been demonstrated in various applications, such as biomedicine, intelligent robots, and human–machine interface.[1–4] Numerous endeavors are implemented to achieve superior performance with high sensitivity, area scale, high spatial resolution, fast response, and wide detect range of tactile sensor via conventional physical transduction mechanisms including piezoresistivity and capacitance.[5–14] Especially, to mimic various perceived capabilities of human skin, tactile sensors with multifunctionalities are investigated to perceive all kinds of external stimuli such as strain, pressure, temperature, and humidity, playing an essential role in smart and interactive flexible/stretchable electronic.[15–19] Recently, a skin-inspired multifunctional sensing matrix which can successfully sense temperature, in-plane strain, humidity, light, magnetic field, pressure, and proximity, has been demonstrated.[20]

Although momentous advancements for pursuing high performance of tactile sensors have been achieved via employing the micro-/nanoscale fabrication and integration technology based on those traditional transduction mechanisms, the capability of tactile sensors to operate independently and sustainably is still needed to be vested.[21] For certain application circumstances, such as implanted or embedded devices for biomedical therapy, healthcare, or nation security monitoring, the mobile or sustainable sensors are crucial and indispensable options. However, the most limitation of traditional tactile sensors lies in the demand

J. Tao, Prof. R. Bao, Prof. X. Wang, Y. Peng, J. Li, S. Fu, Prof. C. F. Pan, Prof. Z. L. Wang
CAS Center for Excellence in Nanoscience
Beijing Key Laboratory of Micro-Nano Energy and Sensor
Beijing Institute of Nanoenergy and Nanosystems
Chinese Academy of Sciences
Beijing 100083, P. R. China
E-mail: baorongrong@binn.cas.cn; cfpan@binn.cas.cn; zlwang@mse.gatech.edu

J. Tao, Prof. R. Bao, Prof. X. Wang, Y. Peng, J. Li, S. Fu, Prof. C. F. Pan, Prof. Z. L. Wang
School of Nanoscience and Technology
University of Chinese Academy of Sciences
Beijing 100049, P. R. China

Prof. R. Bao, Prof. C. F. Pan, Prof. Z. L. Wang
Center on Nanoenergy Research
School of Physical Science and Technology
Guangxi University
Nanning, Guangxi 530004, P. R. China

Prof. C. F. Pan
College of Optoelectronic Engineering
Shenzhen University
Shenzhen 518060, China

Prof. Z. L. Wang
School of Materials Science and Engineering
Georgia Institute of Technology
Atlanta, GA 30332-0245, USA

The ORCID identification number(s) for the author(s) of this article can be found under https://doi.org/10.1002/adfm.201806379.

DOI: 10.1002/adfm.201806379

for external power suppliers almost provided by the rigid batteries, which will suffer from frequently charging and replacement due to the limited life span.[22–25] At the same time, the heavy weight and bulky occupation of batteries also hinder the integration of network system, resulting in the difficulty in usability and portability. Hence, with an increasing number of sensor nodes which are acquired to be put into closed location beyond access, to establish a self-powered tactile sensor network system which can work sustainably without any other external supplier is of great significance in further wearable or implantable devices. So far, lots of studies on self-powered sensor system have been investigated to harvester energy from our environment, such as solar cell for harvesting solar energy based on the photovoltaic effect,[26–29] thermal harvestor for collecting thermal energy based on thermoelectric effect,[30,31] and piezoelectric nanogenerators (PENGs) and triboelectric nanogenerators (TENGs) for gathering mechanical energy based on piezoelectric effect and triboelectric effect.[32–39]

Among these power sources, mechanical energy is considered as one of the most available and attainable power in our daily life, because it is ubiquitous energy source which can be found anywhere and anytime compared with solar energy which depended on the season or weather.[40,41] Therefore, harvesting ambient mechanical energy from ambient environment offers a potential alternative to settle the problem mentioned above. Fortunately, developed by Wang and Song, the first PENG fabricated with on ZnO nanowire–based piezoelectric effect comes out in 2006,[42] which can harvest mechanical energy and convert it into electricity. Based on piezoelectricity, numerous self-powered tactile sensor arrays that can map the pressure distribution with high sensitivity and spatial resolution are demonstrated.[43–48] Subsequently, the newly arising TENG is invented based on triboelectric effect in 2012,[49] which offers a novel technology for harvesting mechanical energy from ambient environment and converting it into electricity. Numerous commendable works are newly demonstrated to harvest all kinds of mechanical energy by TENGs with various structures, such as human movement,[50] wind,[51] blue ocean energy,[52–55] and vibration energy.[56,57] For instance, lawn-structured TENGs are fabricated to scavenge natural wind at arbitrary blowing direction on rooftops.[51] Additionally, a network of TENG is fabricated by Li et al. to efficiently harvest the huge quantities of blue energy from ocean, where the contact and separation occur in the interface of solid and liquid.[53] In spite of acting as an energy harvestor, the produced electrical signals can be the transduction mechanism for the construction of self-powered sensors system.[58] A one-stop self-powered implantable triboelectric sensor which can provide continuous monitoring of multiple physiological and pathological signs are fabricated by Ma et al.[59] Reported by Guo et al., a self-powered auditory sensor for an external hearing aid in intelligent robotic applications is fabricated.[60] Additionally, a fully elastic and metal-free tactile sensor based on TENG, which can detect both normal and tangential forces is proposed by Ren et al.[61]

In this review, progress of self-powered tactile sensor array system based on triboelectric effect will be systematically summarized. First, the fundamental principle of triboelectric effect and the device design are discussed. Performance and functionality are considered as two core development routes, based on which the specific details of tactile sensor system aimed at achieving highly comprehensive performance will be unfolded. Primarily, the development of tactile sensor unit in terms of

Juan Tao received her undergraduate degree from the China University of Geosciences (Beijing) in 2015. Currently, she is pursuing her Ph.D. under the supervision of Prof. Caofeng Pan at the Beijing Institute of Nanoenergy and Nanosystems, CAS. Her research is mainly focused on self-powered systems and flexible pressure sensor devices, and their applications in human–machine interface.

Caofeng Pan received his B.Sc. degree (2005) and his Ph.D. (2010) in Materials Science and Engineering from the Tsinghua University, China. Then, he joined the group of Prof. Zhong Lin Wang at the Georgia Institute of Technology as a postdoctoral fellow. He is currently a professor and a group leader at the Beijing Institute of Nanoenergy and Nanosystems, Chinese Academy of Sciences since 2013. His research interests mainly focus on the fields of piezotronics/piezophototronics for fabricating new electronic and optoelectronic devices, nanopower source, hybrid nanogenerators, and self-powered nanosystems.

Zhong Lin (Z. L.) Wang is the Hightower Chair in Materials Science and Engineering and Regents' Professor at Georgia Tech, the Chief Scientist and Director of the Beijing Institute of Nanoenergy and Nanosystems, Chinese Academy of Sciences. His discovery and breakthroughs in developing nanogenerators and self-powered nanosystems establish the principle and technological roadmap for harvesting mechanical energy from environmental and biological systems for powering personal electronics and future sensor networks. He coined and pioneered the field of piezotronics and piezophototronics.

two main modes including vertical contact–separation mode and single-electrode mode is summarized. Subsequently, we highlight the progress of tactile sensor array for pressure mapping based on triboelectric effect and integration with other mechanisms. Then, two main aspects of systematic applications including human–machine interface and trajectory monitoring will be concentrated on illustrating great potential in practical application. Additionally, the future perspectives of self-powered tactile sensor system based on triboelectric effect are also discussed.

2. Basic Mechanism and Device Design

Although the triboelectric effect has already been known, the positive applications are always ignored and omitted before the invention of TENGs. In this section, the fundamental principle of triboelectric effect and TENGs will be profoundly introduced, in which the charge transfer is regarded as the vital process. Then, on the basis of the working mechanism of TENGs, the device design of self-powered tactile sensor will be introduced.

2.1. Fundamental Principle of Triboelectric Effect

It is well-known that the triboelectric effect also called contact electrification has been discovered since the ancient Greek era of 2600 years ago. Naturally, triboelectric effect as one of the most frequently experienced effects occurs in any two different materials, exhibiting its universality and prevalence. Citing a classical example, as shown in **Figure 1**a, when the hard rubber rod is contacted with a piece of fur through friction, positive charges and negative charges are in equal quantity in the rod and fur due to the neutral substance initially. Then, the rubber rod and fur get negatively charged and positively charged, respectively, due to the occurrence of charge transfer. In the aforementioned case where the material is contacted with a different material through friction, they all get electrically charged when separated, called triboelectric effect.[62] Additionally, when a kind of material which has strong triboelectric effect tends to be insulated or less conductive, the transferred charges could retain on its surface in an extended period of time.[63] In the past 1000 years, this phenomenon is considered as a negative effect blocking development of our community due to the creating electrostatic hazard. Fortunately, TENGs are demonstrated based on the coupling of the triboelectric effect and electrostatic induction, which offers a novel technology for harvesting mechanical energy from ambient environment into electricity.[62] Newly proposed by Wang,[64] it indicates that our nanogenerators are the applications of Maxwell's displacement current in energy and sensors. And, the study also presents that the three major applications of nanogenerators should lie in micro-/nanopower source, self-powered sensors, and blue energy.

Although the essential process of triboelectric effect is ascribed to charge transfer, the specific fundamental understanding of the mechanism still remains to be explored.[62] Especially, the puzzle about the kind of charge species transferred in contact–separation process of the interface is still elusive, and the reason why the transferred charges can be maintained on the surface for a long time without a quick dissipation is hard to be reasonably explained.[65] There are two major types of mechanism: electron transfer and ion transfer. When explained by ion transfer for the most circumstances polymers involved, mobile ions should be contained,[66] or hydronium and hydroxide ions which are ascribed to water from the humid atmosphere work will be involved.[67] However, the electrification between metal and metal, semiconductor, and insulator usually are explained by the electron transfer mechanism.[68] A research developed by Zhou et al.[69] has found that the sign of the transferred charges in contact electrification can be reversed by applying an external electric field. Furthermore, a report conducted by Lu et al.[70] demonstrates that the output performance of TENG will decrease with the increase of temperature. Based on those studies, a research about real-time quantitative measurement of the surface charge amount in triboelectric effect process is newly conducted by Wang and co-workers, which highlights that the transfer mechanism of the contact separation in triboelectric effect process is dominated by electron transfer for the case of solid–solid contact.[65] Furthermore, an electron cloud/potential model based on essential electron cloud interaction is proposed, as shown in Figure 1b. The electron clouds are constructed by the electrons, which spatially surrounded the specific atom or molecule and occupied given orbitals. Thus, a potential well representing an atom can be built and obtained with the out shell electrons loosely bounded. For materials A and B, at the initially separated state, the electrons are trapped, respectively, because of the corresponding potential wells. Once the two materials get into contact with each other, their electron clouds are involuntarily interacted by forming an overlap, yielding an asymmetric double-well potential. At the same time, the electron will jump from the atom of material A to material B, which is the core process of the charge transfer in contact separation process of the triboelectric effect. When the two materials are in physical separation, the transferred charges from material A to material B will be trapped in the potential well again due to the existence of energy barrier of material B under the circumstance that the environmental temperature T is not too high, causing material A positively charged and material B negatively charged. Obviously, the temperature would not be too high normally in our daily life, which is the reason why transferred charges can be retained on the material surface for an extended time without quick dissipation. When the temperature is elevated, the larger energy fluctuations of electrons with the increase of temperature will augment the probability of electrons escaping out of the potential well, facilitating the dissipation of transferred charges of surface.[65,70] It will be noted that the mechanism of the proposed electron cloud model is dominant by electron transfer, but also potentially along with a small proportion of the ion transfer or material transfer.[65] In conclusion, greater endeavors should be given to construct a comprehensive mode to excavate the intrinsic transfer mechanism, which will be adaptive to contact–separation process of all materials to the largest extent. Despite the specific mechanism of the triboelectric effect, various positive applications also should be concerned, in which a self-powered tactile sensor array system based on triboelectric effect will be summarized and focused on.

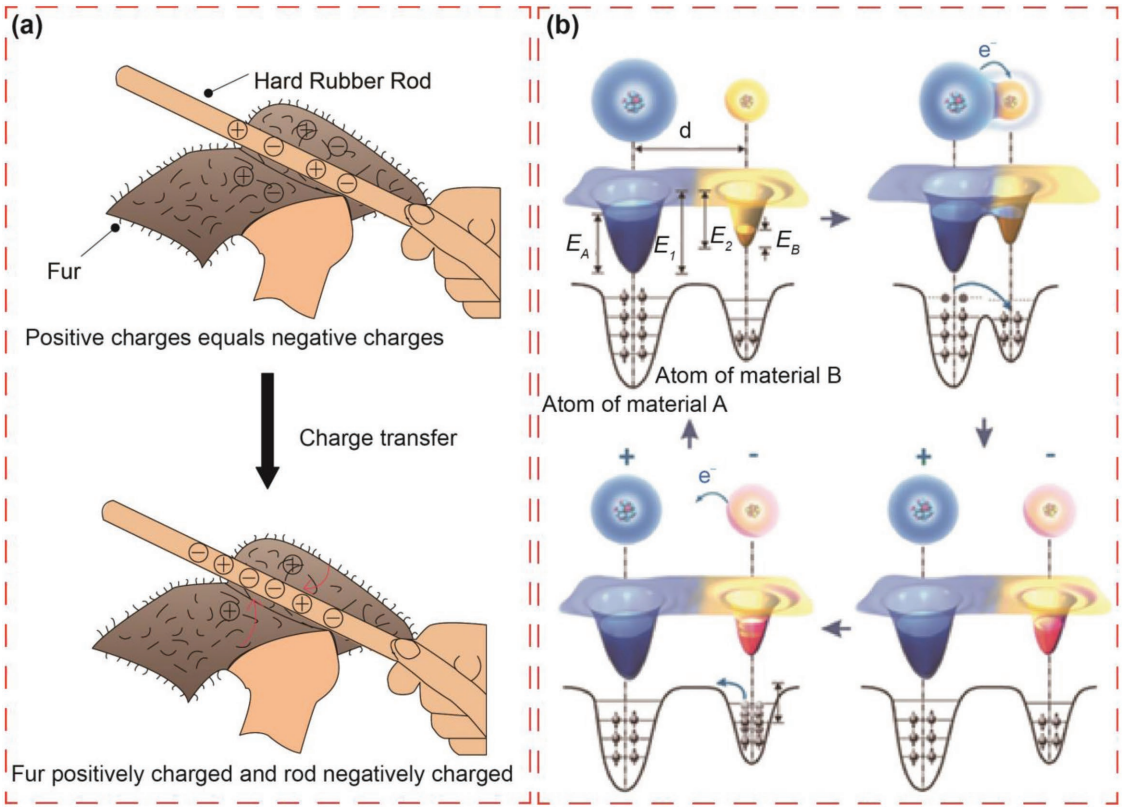

Figure 1. a) Schematic of triboelectric effect phenomenon. b) Schematic of an electron-cloud–potential-well model profile (3D and 2D) proposed for explaining triboelectric effect and charge transfer. Panels b) reproduced with permission.[65] Copyright 2018, Wiley-VCH.

2.2. Device Design of Tactile Sensor Based on Triboelectric Effect

TENGs based on triboelectric effect can not only harvest all kinds of energy and convert it into electricity acting as energy collector, but also enable it to construct a self-powered system serving as various active sensors. A tactile sensor is essentially a transducer which transforms physical stimuli including touch or a certain pressure into measurable and recordable electric signals.[2,3] According to the fundamental working principle of the TENGs mentioned above, the output electrical signals are directly concerned with the external stimulation, in which a relatively larger external force resulted in more transfer charge density due to an intimate contact, achieving a higher output signal.[22,35] Thus, the most immediate application of TENGs should be acting as a tactile sensor to detect external force or touch, and the sensor array for pressure mapping.

In this review, the device designs of tactile sensor based on triboelectric effect will be unfolded in the following two orientations: performance and multifunction, as the profile shown in **Figure 2**. For a self-powered tactile sensor system on the basis of triboelectric effect, the essential performance of high sensitivity, fast response time, high resolution, and wide detection range are the vital factors for guaranteeing the elementary function well for sensing tiny pressure precisely and high resolution mapping matrix.[71–73] On the other hand, the multifunction, such as stretchability, transparency, biocompatibility, self-healing, or conformable properties are considered as the significant factors when applied in practical application simultaneously.[74–76] According to the summary of relevant researches, some approaches are available to enhance the basic performance of tactile sensor system. For instance, micro-/nanostructures on the surface of triboelectric materials such as nanowires or arrays,[72,77] and hierarchical structure between contact materials such as interlocked structures and bulk spacers,[78,79] are utilized to improve the performance of sensor unit. The structure configuration of pixels in the array and versatile processing technology are employed to optimize the spatial resolution of mapping and scalable-area property.[71,73] At the same time, functional materials are adopted to realize the various functional characteristics.[80–83] The progress of the basic tactile sensor unit and array will be summarized from these two aspects toward high sensitivity and resolution, stretchability, transparency, etc., to enhance the comprehensive performance, with the corresponding detailed expression embodied in the following sections.

Surface topography physical modification is a crucial approach which not only can be utilized to boost the triboelectric effect by effectively enhancing contact area between two materials, but also can elevate the detection sensitivity, response, and range of tactile sensor.[78] Different representative materials with various micro-/nanostructural morphologies are created to fortify surface roughness to increase the effective contact area, enhancing the triboelectric effect.[63] At the same time, those micro-/nanostructures are conducive to the enhancement of the sensitivity of tactile sensor by providing a large variation of gap distance between two opposing surfaces,

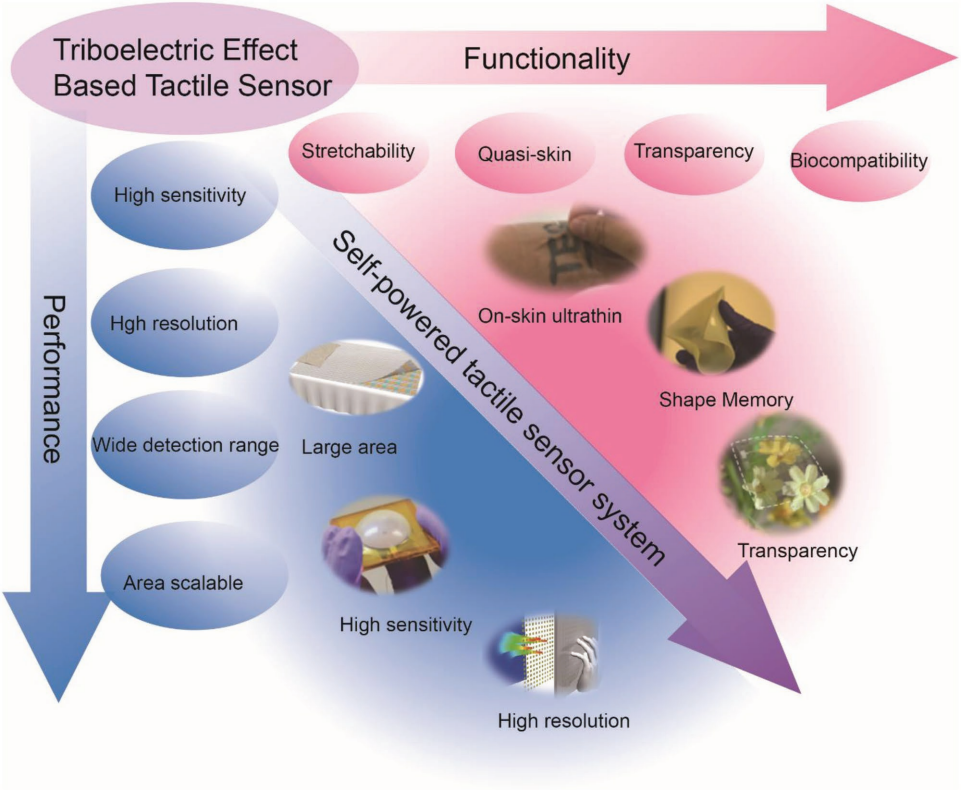

Figure 2. Schematic diagram of device design of triboelectric effect–based tactile sensor from two main aspects: performance and functionality. "Large area" Reproduced with permission.[71] Copyright 2017, Wiley-VCH. "High sensitivity" Reproduced with permission.[72] Copyright 2014, Wiley-VCH. "High resolution" Reproduced with permission.[73] Copyright 2016, Wiley-VCH. "Transparency" Reproduced with permission.[74] Copyright 2018, Wiley-VCH. "Shape memory" Reproduced with permission.[75] Copyright 2018, Wiley-VCH. "On-skin ultrathin" Reproduced with permission.[76] Copyright 2017, Wiley-VCH.

which is proportional to the triboelectric output voltage.[84] For the flexible polymer-based triboelectric materials, vertically aligned nanowire (NW) arrays are commonly employed on the uncovered polymer surface via a top-down approach, such as plasma dry etching or inductively coupled plasma.[72,85] Seen in **Figure 3**a, the fluorinated ethylene propylene (FEP) and polytetrafluoroethylene (PTFE) composed of large percentage of fluorine, are the most triboelectric negative materials with a tendency to gain electrons and widely used for TENG fabrication.[86–88] The created FEP NWs which possess diameter and extend of ≈150 nm and 1.5 µm, can result in a highly sensitive tactile sensor in low pressure detection region due to a more conformable interaction.[85] When compared with bulk FEP film, the easy deformation of NWs facilitates the increment of the real friction area corresponding to an augment of the applied external force. Followed by the similar technique, the scanning electron microscope (SEM) image of PTFE NWs exhibits that the average diameter and length are about 110 nm and 0.8 µm, respectively, facilitating the intimate contact with another material nylon due to the conformable interaction.[89] For stretchable elastomer triboelectric material, polydimethylsiloxane (PDMS) acts as one of the most commonly used silicone materials for fabrication because of its good extensibility and transparency, whose surface can often be modified with regular structures, with SEM shown in Figure 3b. In order to obtain PDMS patterned with pyramid, a corresponding solid Si wafer mold which is initially treated with trimethylchlorosilane for PDMS film stripping from the master easily, is fabricated by photolithography method and wet etching process to gain recessed pyramids.[90] Then, PDMS liquid elastomer is spin-coated on the surface of the mold, and a PDMS film with regular pyramid will be peeled off after curing thermally. Of course, other different structures such as lines and cubes also can be realized by the same technique and fabrication process.[90] Furthermore, a hierarchical nanoporous and microridge PDMS structured of with gradient elastic modulus is proposed to enhance compressibility and contact areal differences due to effective transmission of the external force, resulting in a highly sensitive sensor.[78] For metal thin films acting as dual roles of triboelectric materials and electrodes simultaneously, they are also employed with micro-/nanostructures to boost the surface roughness, as illustrated in Figure 3c. Aluminum (Al) electrode is decorated with the mixture of Ag NWs and nanoparticles (NPs), which is utilized to improve the triboelectric effect as well as pressure response and sensitivity via enhancing effective contact area.[77] Cubic patterns on Al surface are also set up by a typical photolithography process to enhance triboelectric effect.[91] Furthermore, nanopore distributions on the surface of Al are created by electrochemical anodization method, and the enhancement of the effective contact will be realized by the deformation and fill into the vacant nanopores when contacted with another polymer thin film under external force.[86]

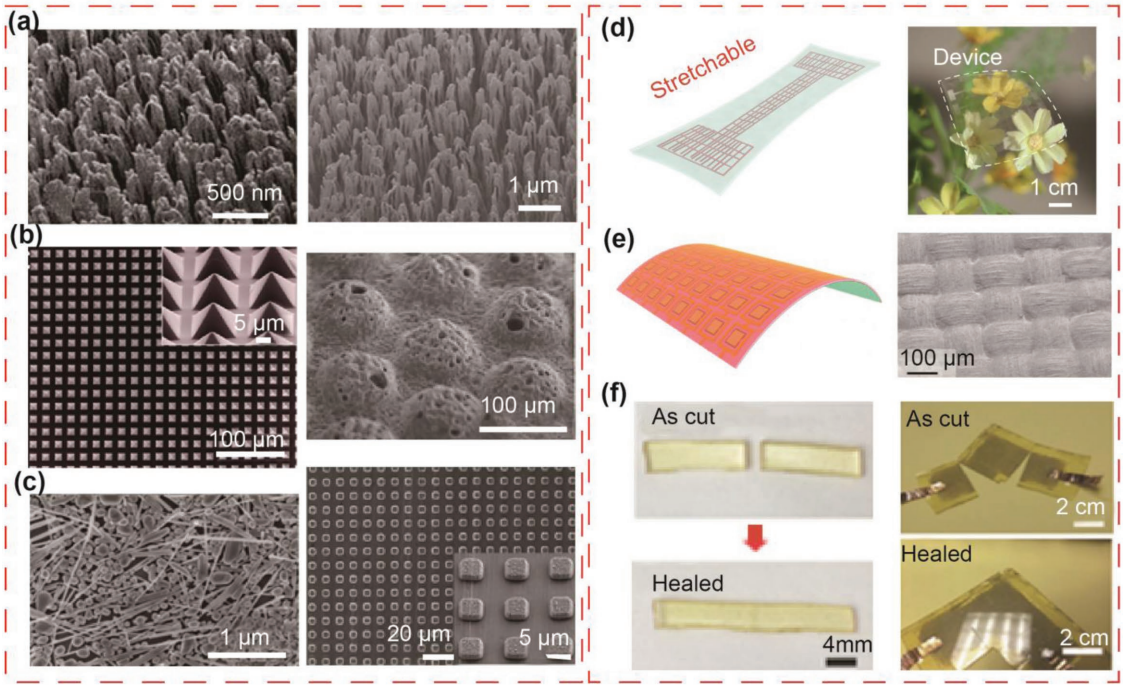

Figure 3. Device design of a triboelectric effect–based tactile sensor. Various surface modifications for enhancing performance: a) polymer-based: FEP and PTFE with NWs. Left: adapted with permission.[85] Copyright 2014, American Chemical Society. Right: adapted with permission.[89] Copyright 2015, Wiley-VCH; b) elastomer-based: PDMS with pyramids and nanoporous and microridge structures. Left: adapted with permission.[90] Copyright 2012, American Chemical Society. Right: adapted with permission.[78] Copyright 2018, American Chemical Society; c) electrode-based: Ag NWs and NPs, Al with cubic patterns. Left: adapted with permission.[77] Copyright 2013, American Chemical Society. Right: adapted with permission.[91] Copyright 2012 American Chemical Society. Various materials for realization of functionalization: d) stretchable and transparent PDMS with Ag NWs. Reproduced with permission.[68] Copyright 2018, The Royal Society; e) area scalable textile-based. Reproduced with permission.[101] Copyright 2017, Elsevier Ltd.; f) self-healable vitrimer elastomer-based. Reproduced with permission.[80] Copyright 2018, Wiley-VCH.

With the rapid development of internet of things, functionalization of electronics with stretchable, transparent, quasi-skin, and biocompatible characteristics mimicking the unique properties of electronic skins, have received extensive attention for the alternative next-generation electronics. Primarily, in order to achieve the stretchability of TENG, the most direct way is to choose triboelectric materials of elastomer with low Young's moduli and intrinsic elasticity, like commonly used PDMS, Ecoflex, and silicon rubber. However, the back electrode of triboelectric materials of elastomer should also possess extensibility in the case of maintaining an excellent conductivity. Thus, coupled with triboelectric materials of elastomer, those electrode materials, such as carbon nanotube (CNT) mixture and conductive liquid with stretchability,[83,92,93] Ag NWs and hydrogel with both stretchability and transparency,[81,94] are employed for the fabrication of TENG to realize stretchability. Our group has developed a highly stretchable and transparent self-powered tactile sensor based on triboelectric effect with patterned Ag-nanofiber electrodes on PDMS, which is demonstrated with high transparency larger than 70%, low sheet resistance of 1.68–11.1 Ω^{-1}, and excellent stretchability (Figure 3d).[74] Certainly, geometrical structures such as wavy Kapton film and kirigami paper are also employed to further enhance stretchability and adaptability.[95,96] Additionally, with the arrival of electronic-textile or smart textile era, the flourishing trend of self-powered textile-based TENG is demonstrated to satisfy the wearable, washable, and area-scalable characteristics.[71,97–100] A recent work about textile-based self-powered triboelectric touch sensor array is pioneered, in which the top layer electrification material is made of PTFE textile and electrodes are essentially fabricated with woven fabric deposited with copper and nickel, with the devices capable of easily being bent, rolled, and scalable in area (Figure 3e).[101] Even more, based on textile, triboelectric tactile sensor with designable CNT ink electrodes by screen print has been put forward to own the washable and breathable properties. Apart from stretchable, transparent, and wearable capabilities mentioned above, TENGs with more novel function mimicking human skin such as self-healing (Figure 3f), shape-memory, and biodegradable properties are initiated in recently years, which offer an environmentally friendly superexcellent entrance for implantable medical, electronic skin, and smart sensor system.[75,76,80,82,102]

3. Self-Powered Tactile Sensor Based on the Triboelectric Effect

Motivated by abovementioned working principle of the TENGs, the most fundamental and immediate application lies in the tactile or pressure sensor because the output electrical signals of TENGs are greatly influenced by magnitude/frequency of the external force. In this respect, TENGs play a dual role in both providing an autonomous power source without any other power consumption and serving as a tactile sensor for

monitoring external stimulation with the output signals as a transducer. Herein, the development of triboelectric tactile sensor unit will be summarized. Furthermore, self-powered tactile arrays are established to achieve pressure mapping/imaging which exhibit high sensitivity and spatial resolution, wide detect range, and low power consumption. Moreover, triboelectric effect which is integrated with other mechanisms like mechanoluminescence, transistor, and electroluminescence is utilized to optimize the performance, such as widening the detection pressure range and visualizing the tactile mapping.

3.1. Tactile Sensor Unit

Up to now, in spite of diverse configurations employed in collecting multifarious mechanical energy in complicated circumstances, TENGs are divided into four principal types consisting of vertical contact–separation mode, lateral sliding mode, single-electrode mode, and freestanding triboelectric-layer mode.[40] Among these modes, the vertical contact–separation mode and single-electrode mode with their own unique characteristics are the most commonly used approaches to demonstrate the self-powered pressure or touch sense system applications, because the applied external force is vertically applied onto the contact surface in the two modes. Certainly, sliding mode is occasionally combined with single-electrode mode in tactile sensor system to realize various monitorings of motion trajectory, which will be explained and reviewed in application system section. Additionally, the development of tactile sensors based on triboelectric effect is summarized in terms of the working mode, triboelectric materials, and the performance including sensitivity, detection range, linearity, response time, and limit of detection, as illustrated in **Table 1**.

3.1.1. Tactile Sensor Based on Vertical Contact–Separation Mode

The vertical contact–separation mode is the earliest configuration, with the basic working principle illustrated in **Figure 4**a. TENGs based on this mode consists of two films with distinctively different triboelectric polarities in a stacked configuration, at least one of which needs to be dielectric with electrode attached onto its outer surface.[22] Under the external mechanical stimuli, the two triboelectric materials get into mutual contact, generating opposite charges in equal quantity as a result of triboelectric effect at the same time. A significant electric potential difference can be established after releasing, and electrical signals will be detected when the two electrodes are connected through an electrometer. Once the gap distance of two materials decreases again, a reduced potential difference will result in a reversed electrical signal. The first proof-of-concept pressure sensor based on triboelectric effect is proposed by Fan et al.,[90] which is in accordance with the simplest structure of vertical contact–separation mode. Composed of stacking Kapton and polyester (PET), a charge generation, separation, and induction process can be accomplished by a mechanical deformation of the polymer films under the external pressure. This transparent, flexible self-powered pressure sensor with a high sensitivity can sense a tiny pressure of a water droplet (8 mg, ≈3.6 Pa) and a falling feather (20 mg, ≈0.4 Pa) with a detection limit of ≈13 mPa. Followed by a quantitative and comprehensive work reported by Lin et al. (Figure 4b),[77] both a static and dynamic pressure sensing are achieved via different measurement approaches theoretically and experimentally. The triboelectric materials are constituted by PDMS with modified micropatterned pyramid structures and Al film embedded with Ag NWs and NPs which acts as an electrode simultaneously. It is noted that the structure modification on both the triboelectric surfaces is brought in to raise the triboelectric charge density and pressure response simultaneously. Theoretically, the relative variation of the voltage and the applied pressure can be analyzed by the following equation

$$\left(V_{oc,0} - V_{oc}\right) / V_{oc,0} = \left(d_0 - d\right) / d_0 = \left(S / \left(k \cdot d_0\right)\right) \cdot p \tag{1}$$

where V_{oc} is the open-circuit voltage, d is the distance of two layers, p is the pressure, and k represents the elastic property of the material. Hence, the relationship should be expected to a directly linear relationship, providing a credible measuring method for the magnitude of external force.[77] Furthermore, the transferred charge density can be served for detecting static pressure but the relationship presents nonlinearity. The output short-circuit current is influenced by the magnitude and frequency of the external force, and it is defined by the following equation

$$J_{sc} = \mathrm{d}(\Delta\sigma) / \mathrm{d}(t) \tag{2}$$

where σ is the transferred charge. Hence, larger magnitude and faster frequency will result in a higher short-circuit current due to more effective contact area and faster speed, respectively. As a consequence, a dynamic pressure sensing including amplitude and loading rate will be achieved by the current acting as a monitoring parameter. Experimentally, the relationship between relative voltage variation $\Delta V/V_0$ and applied pressure has been displayed, where the slope represents the sensitivity of sensor. Compared with the linear region II for high pressure with the sensitivity of 0.01 kPa^{-1}, the linear region I for low pressure presents a higher sensitivity of 0.31 kPa^{-1} due to a larger increase in contact area and voltage variation for low pressure while an almost saturation of contact area between two materials for high pressure. As for the experimentally dynamic pressure sensing, the rectified current under different applied pressures is discussed under the same loading/unloading frequency of external force in an increasing and decreasing force process. A coincidence between the two curves illustrates the valid basis of short-circuit current as a sensing permanent for applied force. Simultaneously, when keeping the applied pressure as a constant, different rectified currents can be attained under different loading/unloading frequencies. Thus, dynamic sensing of pressure including amplitude and frequency can be accomplished by the current signal. Besides, the response time and the detection limit of the sensor is less than 5 ms and 2.1 Pa, respectively, with the detection range inferred to be less than 14 kPa according to the experimental measurement.

Subsequently, lots of researches about tactile sensor based on vertical contact–separation mode have been investigated

Table 1. Summary of tactile sensors based on triboelectric effect and their performance.

Working modes	Triboelectric materials	Sensitivity	Detection range	Linearity	Response time	Detection limit	Ref.
Vertical contact–separation	PDMS and ITO	Not known	Not known	Not known	Not known	≈13 mPa	[90]
Single-electrode	PDMS (micropyramid)	0.29 ± 0.02 V kPa^{-1}	<10 kPa	Linear	0.1 s	0.4 kPa	[105]
Vertical contact–separation	PDMS and Ag NWs/NP	0.31 kPa^{-1} (<3 kPa) 0.01 kPa^{-1} (3–14 kPa)	Not known	Two consecutive linear regions	<5 ms	2.1 Pa	[77]
Vertical contact–separation	FEP (NWs) and Latex	6.9 V kPa^{-1} (3.1–12.2 kPa)	Not known	Linear	Not known	0.16 Pa	[72]
Vertical contact–separation	Polyline (air voids in layers) and Al	3.0 kPa^{-1} (<30 kPa) 0.7 kPa^{-1} (30–50 kPa)	<50 kPa	Two consecutive linear regions	Not known	Not known	[104]
Single-electrode	FEP (NWs)	44 mV kPa^{-1} (<0.15 kPa) 0.5 mV kPa^{-1} (2–12 kPa)	<12 kPa	Two consecutive linear regions	Not known	Not known	[85]
Single-electrode	PTFE (NWs) and Nylon	51 mV Pa^{-1} (2.5 Pa–1.2 kPa) 3 mV Pa^{-1} (1.2–6 kPa)	<6 kPa	Two consecutive linear regions	Not known	2.5 Pa	[89]
Single-electrode	PTFE (NWs)	0.947 μA MPa^{-1}	<2.5 MPa	Linear	Not known	Not known	[108]
Vertical contact–separation	PDMS (side walls and micropyramid) and ITO	2.82 ± 0.187 V MPa^{-1} (0.3–428.8 kPa)	0.3–428.8 kPa	Linear	≈40 ms	0.30 kPa	[79]
Single-electrode	Graphene oxide	388 μA MPa^{-1} (2.5–125 kPa)	2.5–125 kPa	Linear	Not known	Not known	[107]
Single-electrode	FEP (microstructure)	2.79 mV Pa^{-1} (<1 kPa) 0.2 mV Pa^{-1} (10–70 kPa) 0.03 mV Pa^{-1} (70–250 kPa)	<250 kPa	Three consecutive linear regions	≈50 ms	Not known	[110]
Single-electrode	PDMS (micropyramid)	6 MPa^{-1}	0.6–200 kPa	Linear	50 ms	600 Pa	[112]
Single-electrode	Elastomer (ionic hydrogel)	0.013 kPa^{-1} (1.3–70 kPa)	1.3–70 kPa	Linear	Not known	1.3 kPa	[81]
Single-electrode	Conductive fiber and PET	0.77 V Pa^{-1} (<5.2 kPa) 34.7 mV Pa^{-1}	<14 kPa	Two consecutive linear regions	<80 ms	Not known	[71]
Vertical contact–separation	PDMS (nanoporous) and P(VDF-TrFE)	0.55 V kPa^{-1} (<19.8 kPa) 0.2 V kPa^{-1} (19.8–100 kPa)	<100 kPa	Two consecutive linear regions	Not known	Not known	[78]
Vertical contact–separation	PDMS and CNT	0.35 V kPa^{-1} (5–50 kPa) 0.51 V kPa^{-1} (50–100 kPa) 0.18 V kPa^{-1} (100–200 kPa) 0.04 V kPa^{-1} (200–450 kPa)	5–450 kPa	Four consecutive linear regions	0.45 s	Not known	[103]
Single-electrode	Silk (CNT ink)	0.0479 kPa^{-1} (<100 kPa) 0.0186 kPa^{-1} (100–400 kPa) 0.0033 kPa^{-1} (400–650 kPa)	<650 kPa	Three consecutive linear regions	Not known	Not known	[106]
Single-electrode	Ecoflex rubber (microprism structure)	9.54 V kPa^{-1} (<5 kPa)	<25 kPa	Not known	Not known	63 Pa	[126]
Single-electrode	PDMS (Burr arrays of carbon black)	51.43 V kPa^{-1} (normal force) 0.83 N V^{-1} (0.5–3 N) 2.50 N V^{-1} (3–40 N) (tangential force)	0.1–1.5 MPa 0.5–40 N	Linear Three consecutive linear regions	Not known	Not known	[61]

to improve the performance.[78,79,103,104] Jiang et al. demonstrates a flexible, transparent, and waterproof triboelectric tactile sensor with triboelectric materials of micropyramid-modified PDMS and indium tin oxide (ITO) separated by PDMS side walls, showing a pressure sensitivity of 2.82 ± 0.187 V MPa^{-1}.[79] Recently, a highly sensitive triboelectric tactile sensor is developed by Ha et al. based on the integration of two structure design of hierarchical nanoporous and interlocked microridge-structured polymers (Figure 4c).[78] In the structure design, soft PDMS layer with a low elastic modulus and stiff poly(vinylidenefluoride-cotrifluoroethylene) [P(VDF-TrFE)] layer are utilized as contact materials, inspired by stiff epidermis and soft dermis layers of human skin. Specifically, gradient stiffness structure is aimed at enhancing the compressibility and contact areal differences on account of effective transmission of the external pressure from stiff to soft layers, while nanoporous structures into the interlocked and microridge-structured polymers will result in more effective variation of both volume and gap distance between two friction surfaces without the need of additional bulky spacers. Thus, the combination of these two structures receives the highest triboelectric output performance and pressure sensitivity than other different structures with and without nanoporous and microridge structures. Furthermore, the relationship between the output voltage and different applied pressures under different width (w) and pitch (p) sizes of microridge arrays (w/p = 25/30, 50/60, and 100/120 μm) is explored. The result shows that the triboelectric output voltage enhances with the increasing of width and pitch sizes, as a consequence, the microridge arrays with w/p of 100/120 μm exhibits the highest pressure sensitivity of 0.55 V kPa^{-1} up to 19.8 kPa and

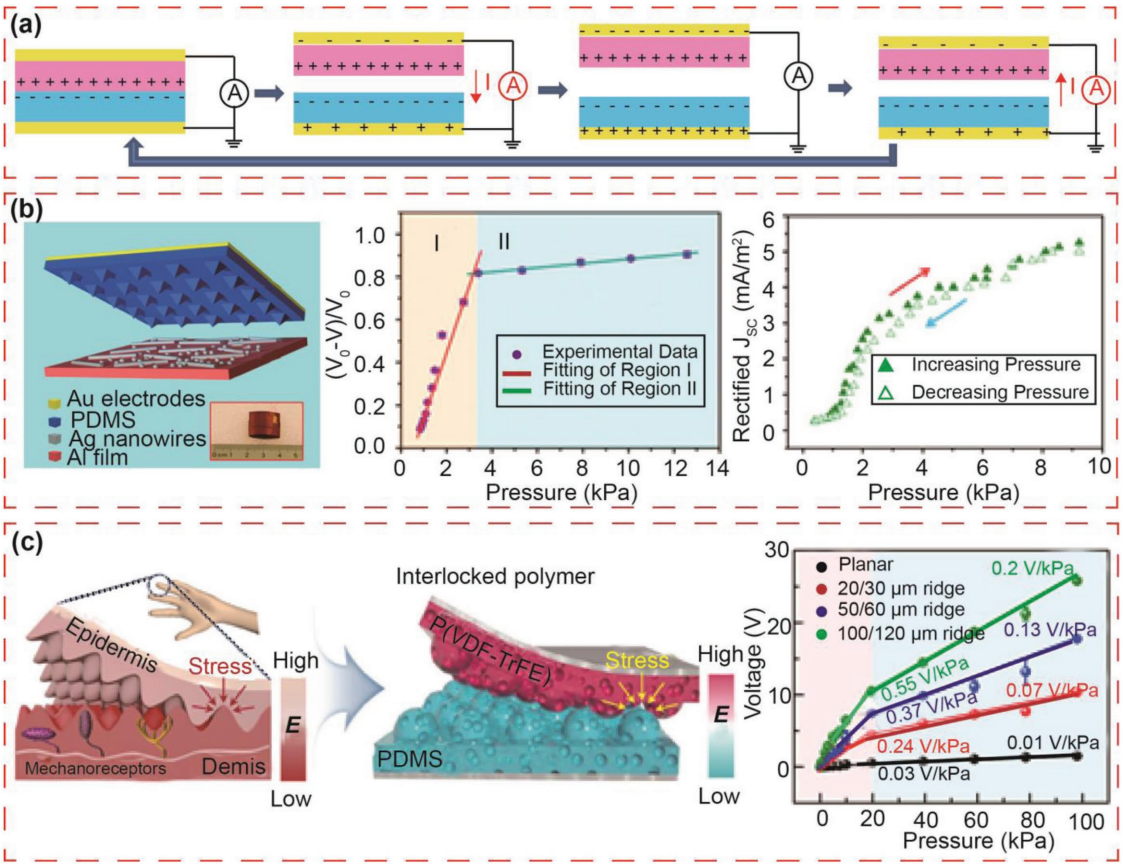

Figure 4. Development of tactile sensor unit based on vertical contact–separation mode. a) The working principle of vertical contact–separation mode. b) Both static and dynamic pressure sensing. Reproduced with permission.[77] Copyright 2013, American Chemical Society. c) Skin-spired pressure sensor based on the integration of two structure design. Reproduced with permission.[78] Copyright 2018, American Chemical Society.

a relative low sensitivity of 0.2 V kPa^{-1} under 100 kPa particularly. This high pressure sensitivity of hierarchical microridge arrays in the low pressure range can be used to monitor weak pulse pressure of radial artery, demonstrating its highly reliable feasibility and practicability in wearable devices for health monitoring. It can be found that the performance and functionality have been enhanced simultaneously with the employment of developed structure design and materials.

3.1.2. Tactile Sensor Based on Single-Electrode Mode

Naturally, assuming that the human skin has an access to participating in touch sensing as a contact material since all objects can be chosen as triboelectric materials, the usage scope will be greatly expanded. Thus, single-electrode mode endows one triboelectric material with the unique property that it can be free or moving object, which provides the great convenience for various circumstances in practical applications, with the fundamental operating principle shown in **Figure 5**a. In single-electrode mode, only one triboelectric layer is fixed in device configuration with the corresponding back single electrode connected to ground as a reference electrode for an electron source. The periodic change of the contact area or gap distance between the fixed material and the moving object can give rise to charge transfer and electrostatic induction, producing the alternate flow of electrons in external circuit. Although, the electrostatic-induced electron transfer in this mode is not the most effective way,[24,25,40] the simplified fabrication way and another free object without restriction are favorable for practical applications in both pressure and touch sensing.

Previously, the first self-powered tactile sensor based on single electrode is demonstrated by Yang et al.,[105] which is realized by the contact and separation between human skin and PDMS through directly harvesting biomechanical energy from the motion of human finger, exhibiting a sensitivity of 0.29 V kPa^{-1} and a response time of less than 0.1 s. Afterward, tactile sensor composed by FEP based on a single-electrode mode with improved performance is proposed by Zhu et al.,[85] as shown in Figure 5b. The device is constructed by a single ITO electrode deposited onto a PET substrate connected to ground, and FEP modified with vertically aligned NWs and moving objects serving as the triboelectric materials. An enhancement tendency in output voltage has been attained with the increasing of applied external force which is ascribed to the reduced gap distance and increased contact area. Two distinct linear regions with a fast increasing initially and a slow increasing subsequently are presented. For the extremely low-pressure region I less than 0.15 kPa, an extraordinary sensitivity of 44 mV Pa^{-1} is received with preferable linearity (R^2 = 0.991). While the

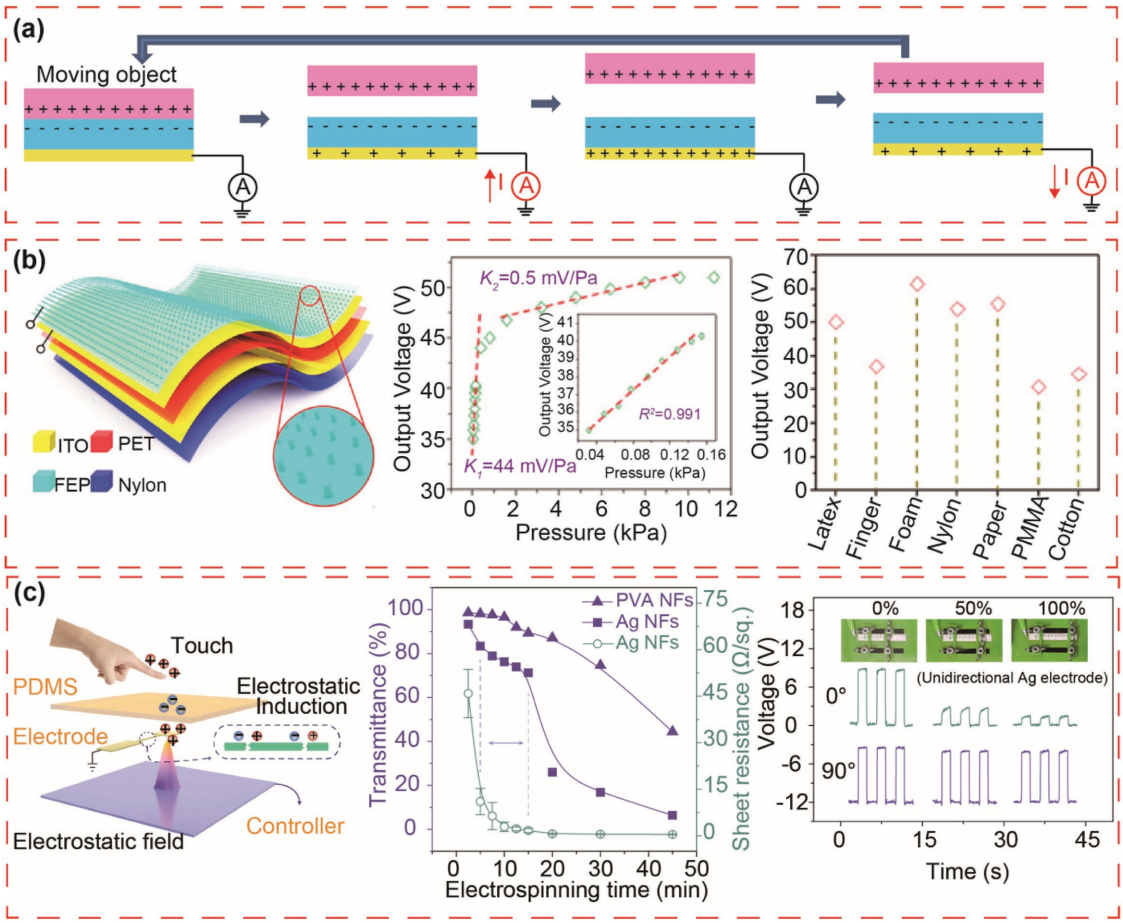

Figure 5. Development of tactile sensor unit based on single-electrode mode. a) The working principle of on single-electrode mode. b) Flexible ultrasensitive flexible tactile sensor. Reproduced with permission.[85] Copyright 2014, American Chemical Society. c) Highly stretchable and transparent tactile sensor. Reproduced with permission.[74] Copyright 2018, Wiley-VCH.

pressure is beyond 2 kPa in region II, the sensor exhibits a sensitivity of 0.5 mV Pa^{-1} with a good linearity (R^2 = 0.974). The FEP with strong electron affinity capability and the modified NWs with 1.5 µm endow an enhanced triboelectric effect and a high sensitivity of tactile sensor, with a sevenfold enhancement in pressure sensitivity compared with a bulk FEP film. Moderately, shorter NWs of 600 nm will result in an ineffective area with contact object, while the excessively long NWs larger than 3 µm will lead to a poor mechanical robustness. Additionally, on account of its unique property, this kind of tactile sensor based on single-electrode mode has the capability in perceiving different objects made of various textures, which is attributed to the different output voltages in response to diverse triboelectric effects of electron affinity difference. This capability reveals its widespread applicability in a variety of circumstances and perception sensing for different materials in e-skin and human–machine interaction. In order to optimize its comprehensive performance, more efforts are exerted to climb the high performance and multifunction. A self-powered tactile sensor based on single-electrode mode composed by textile and CNTs by screen-printing technology is proposed, with the wide detection range to 700 kPa.[106] The linear regions with different sensitivities can be divided into three regions, including 0.0479, 0.0186, and 0.0033 kPa^{-1}. The optimized performance can be attributed to the rough surface constituted of numerous microfibers of textile and CNTs. Furthermore, in this mode, various materials such as graphene oxide and conductive fiber are used for tactile sensors to improve the comprehensive properties.[71,107,108]

Recently, our group put forward a self-powered triboelectric tactile sensor consisting of the high stretchable and transparent patterned Ag nanofiber (Ag NF) electrodes by electrostatic spinning on the elastomeric PDMS substrate,[74] as shown in Figure 5c. Due to the stronger electron affinity of PDMS than that of finger, electrons will transfer from finger to PDMS, yielding PDMS negatively charged. Under periodic stimulus of touch and removal of the finger, the electrical signals will be received regularly, revealing its feasibility of tactile sensing. The optical transparency and electrical conductivity of the electrodes are investigated by analyzing the transmittance spectra and sheet resistance. The results reveal that when the electrospinning time ranges from 5 to 15 min, the sheet resistance ranges from 11.1 to 1.68 Ω^{-1} with an excellent transmittance larger than 70%, confirming a superior performance as a transparent conductive electrode of tactile sensor. Furthermore, the stretchability and durability are measured for practical applications in stretchable tactile sensors. Tactile sensor based on unidirectional

Ag NF electrodes exhibits an inferior tensile property. On the contrary, the output voltage of the tactile sensor based on bidirectional unidirectional Ag NF electrodes remains unaltered, demonstrating a remarkable stretchability. In addition to the normal pressure detect, a tactile sensor based on single-electrode mode which can detect both normal and tangential forces has been recently demonstrated.[61] The tiny arrays of carbon black on the contact surface are prepared to facilitate the elastic deformation, which largely promotes the pressure detection range up to 1.5 MPa and sensitivity of 51.43 V kPa^{-1}. Simultaneously, the sensor can detect tangential forces from 0.5 to 40 N, with a relatively rough sensitivity of 0.83 N V^{-1} in the range of 0.5–3 N and 2.50 N V^{-1} in the range of 3–40 N.

3.2. Tactile Sensor Array

Under the development of the tactile sensor mainly based on vertical contact–separation mode and single-electrode mode mentioned above, tactile sensor array, which is the integration of the sensor unit assembled together, has been demonstrated for touch imaging and pressure mapping. Because restricted resolution is limited by the structure design of vertical contact–separation mode, more attentions and endeavors have been exerted on the tactile sensor array based on single-electrode mode to improve the spatial resolution. Moreover, to achieve high performance, self- powered tactile sensor array based on triboelectric effect integrated with other mechanism also has been discussed, especially with mechanoluminescence, transistor, and electroluminescence to obtain full dynamic-range detection, drain–source current modulation, and electroluminescence.

3.2.1. Array of Tactile Mapping Based on Triboelectric Effect

Initially, the first tactile sensor array based on triboelectric effect is promoted by Lin et al.,[77] which is fabricated on the vertical contact–separation mode by integrating 6 × 6 separated sensor unit onto the same grounded electrode. Once some pixels are exerted by applied pressure, the voltage signals will be observed in these pixels, while other profile of pixels still remains constant synchronously, thus the letter "TENG" is spatially imaged with distinguishable profile. Afterward, a light-emitting diode (LED)–TENG tactile matrix with the 8 × 7 pixels is proposed to visualize the pressure mapping by recording the electroluminescent signals of the LEDs without external power source, in which the magnitude of applied pressure is characterized by light emission density of the LED.[104] However, the integration method of this kind vertical contact–separation mode is not suitable for the large-scale fabrication with high-resolution arrays because each pixel is packaged independently in the matrix. Compared with vertical contact–separation, the tactile array based on single-electrode mode provides a better integration way to potentially obtain high resolution, demonstrating the advantages of a simple device design and preparation method.[109] The tactile array based on single-electrode mode is first proposed by Yang et al.,[105] in which the triboelectric material PDMS is intact with ITO electrodes separated to fabricate array configuration. In other words, the active size depended on the size of each electrode patch, which can be significantly reduced by various microfabrication and sophisticated design in the device structure.

Improved by Wang et al.,[73] on the basis of single-electrode mode, a self-powered, high-resolution, and pressure-sensitive triboelectric tactile sensor array capable of enabling real-time tactile mapping is demonstrated. First, the structure fabrication of tactile sensor matrix based on single-electrode mode is illustrated in **Figure 6**a, with a PDMS film spin-coated onto the top serving as the electrification layer. The top PET with a thickness of 25 µm severs as a flexible substrate, where the deposited Ag electrode array presents aligned on the top serving as the charge-sensing element and the circuit configuration electrodes on the back side are connected to the external measuring equipment. Another bottom PET film coated with ethylene–vinyl acetate copolymer (EVA) is utilized as an encapsulation layer of the circuit configuration electrodes. In this configuration and structure design, a 16 × 16 pixelated triboelectric sensor matrix with a resolution of 5 dpi is demonstrated with the side length of each pixel 2.5 mm, with the corresponding schematic of the pressure mapping process shown in Figure 6b. As for the data acquisition for multipixels synchronously, an available multichannel data acquisition method is adopted to realize the combination of large-scale data processing and real-time tactile imaging. The simulated results of potential distinction between the touched and untouched electrodes can be observed clearly under the touch sensing of unipoint, bipoints, and multipoints, theoretically verifying the feasibility and validity of multipoint touch sensing. When applying an external force on the top of the tactile array by a mold in the shape of number "6," a facile and explicit imaging of the mold shape can be exhibited via an experimental mapping profile according to the output voltage signals of simultaneous use of multiple pixels. Furthermore, in order to increase the pixels and enlarge the scale of the sensor matrix, the circuit configuration on the bottom side of the device will become more sophisticated and a bulky number of addressing lines ($m \times n$) will put forward further challenges to hinder the fast mapping, which is unbeneficial for the practical device fabrication and data acquisition. Hence, a novel cross-type configuration is developed to overcome the aforementioned challenges by reducing the number of scanning channels to $m + n$ and simplifying the device structure, with the ameliorative electrode structure displayed in Figure 6c. An aligned rhombic array is proposed to improve the effective area ratio in each pixel, where row electrodes are electrically connected to the top surface of the PET substrate, while column electrodes are connected to the backside. On the basis of improved structure design, a 36 × 20 tactile matrix with a pixel resolution of 10 dpi is demonstrated. Facilitating its practical commercial application, the transparent electrode ITO is adopted to demonstrate a simple touch-panel screen, where a touch tracing of a word "3" on the surface of the tactile sensor matrix is depicted in Figure 6d. Additionally, a discernible pressure mapping will be observed (Figure 6e), where the distinct difference in output voltage signals between the touched and untouched pixels verifies the practicability of this self-powered tactile sensor array based on triboelectric effect in human-interactive interfaces for consumer electronics.

Followed by the similar structure design, lots of works are conducted to constructing the triboelectric tactile array

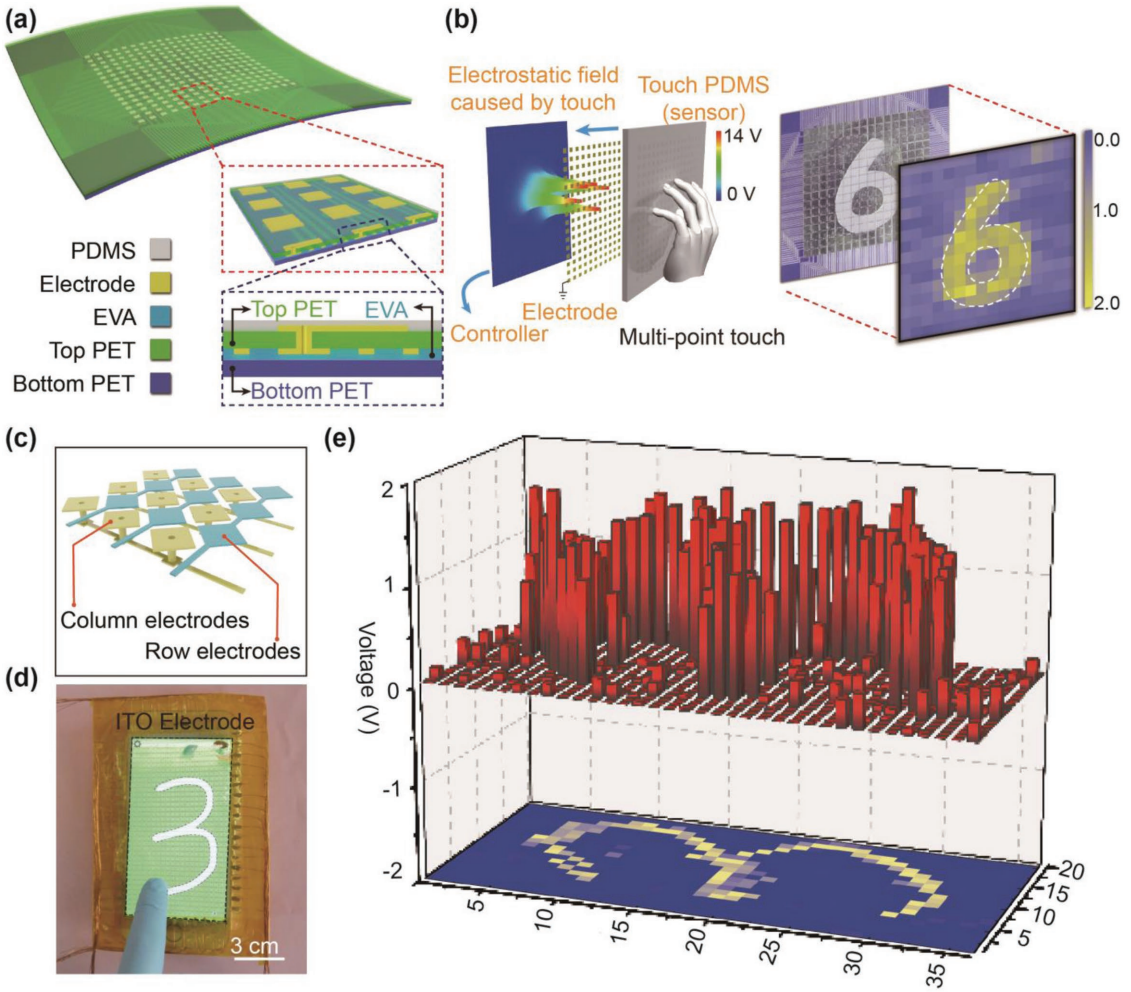

Figure 6. High-resolution and pressure-sensitive triboelectric sensor matrix for real-time tactile mapping. a) Schematic of the device structure of 16 × 16 matrix. b) Schematic diagram of the pressure mapping process. c) Structure design of the cross-type electrode of 36 × 20 matrix. d) Illustration of a cross-type triboelectric sensor matrix attached to a commercial smart phone by monitoring a trail of a "3." e) Diagrams tactile mapping of "3." All panels reproduced with permission.[73] Copyright 2016, Wiley-VCH.

sensing system. A transparent and flexible triboelectric sensing array with fingertip-sized pixels is demonstrated, which can be used in real-time touch sensing, spatial mapping, and motion monitoring.[110] An ultrahigh resolution of 127 × 127 dpi is realized in pressure sensing in terms of output current of each pixel via carbon fibers acting as electrodes.[111] Although, the matrix possessed high resolution due to signal carbon fiber as a row/column electrode, the relatively low sensitivity of 0.055 nA kPa^{-1} and inferior triboelectric effect are presented. Particularly, a self-powered triboelectric sensor array with highly stretchable and transparent properties is fabricated by using the random Ag NF electrodes for tactile mapping.[74] To obtain Ag NF electrodes, various orientations of large-scale polyvinyl alcohol (PVA) NFs are controllably prepared by altering the shape of metal collector by electrostatic spinning, as the schematic diagram in **Figure 7**a. Then, an 8 × 8 transparent stretchable sensor matrix is promoted based on the optimal structure configuration referred before,[73] where the column and row electrodes with a crossbar-type are employed to enhance the mapping rate, as displayed in Figure 7b. Herein, a multiswitch scanning method is adopted to simplify the test system and boost scanning efficiency instead of multi-electrometer scanning mode. The corresponding coordinates have the maximum voltage values in a scanning cycle when a pixel is under applied pressure. As shown in Figure 7c, when pixels of (X4Y7), (X7Y4), and (X4Y2) are touched in turn, the corresponding voltage signals and a real-time tactile mapping will be manifested by data acquisition and software analysis. Finally, a demo of Pac-Man has been presented, with four regions divided for the control of moving direction of up, down, left, and right when the corresponding pixels are touched (Figure 7d).

3.2.2. Array of Tactile Mapping Based on Triboelectric Effect Integrated with Other Mechanisms

Although lots of endeavors have been devoted to elevating the performance of self-powered tactile sensor based on triboelectric effect according to the aforementioned summary,

the wide detection range, high spatial resolution, and visualization still need to be excavated to expand the practical application in e-skin, robots, and human–machine interface. Aimed at improving the detection range, a full dynamic-range pressure sensor matrix is demonstrated by integrating dual mode of triboelectric effect and mechanoluminescent mechanism, exhibiting high sensitivity and resolution at the same time.[112] A large-scale 100 × 100 matrix with a high resolution of 100 dpi is demonstrated to achieve real-time pressure profile detecting and depicting, with the structure schematic shown in **Figure 8**a. Effectively, a crossbar-type electrode and the rhombic array configuration are employed to enhance the mapping rate and effective area ratio in each pixel at a certain resolution in triboelectric sensor matrix (TESM), while the ZnS:Mn powder and photoresist on the top of the electrodes are designed for mechanoluminescent sensor matrix (MLSM). Each MLSM pixel is located in the center of every four TESM pixels to get more light penetration, with spin-coated polymethyl methacrylate (PMMA) serving as a protective layer of MLSM and PDMS with modified microstructure acting as the triboelectric film of TESM, respectively. An excellent pressure sensitivity of 6 and 0.037 MPa^{-1} are attained for TESM and MLSM, respectively, with the corresponding detection range of 0.6–200 kPa and 650 kPa–30 MPa (Figure 8c). It can be observed that a stable output voltage response will be attained under an identical applied pressure for TESM, while the corresponding visible-light optical images are illustrated in different applied pressures, demonstrating the valid reliability of the electrical and optical dual-mode detection. Various potential applications are available based on this full dynamic-range

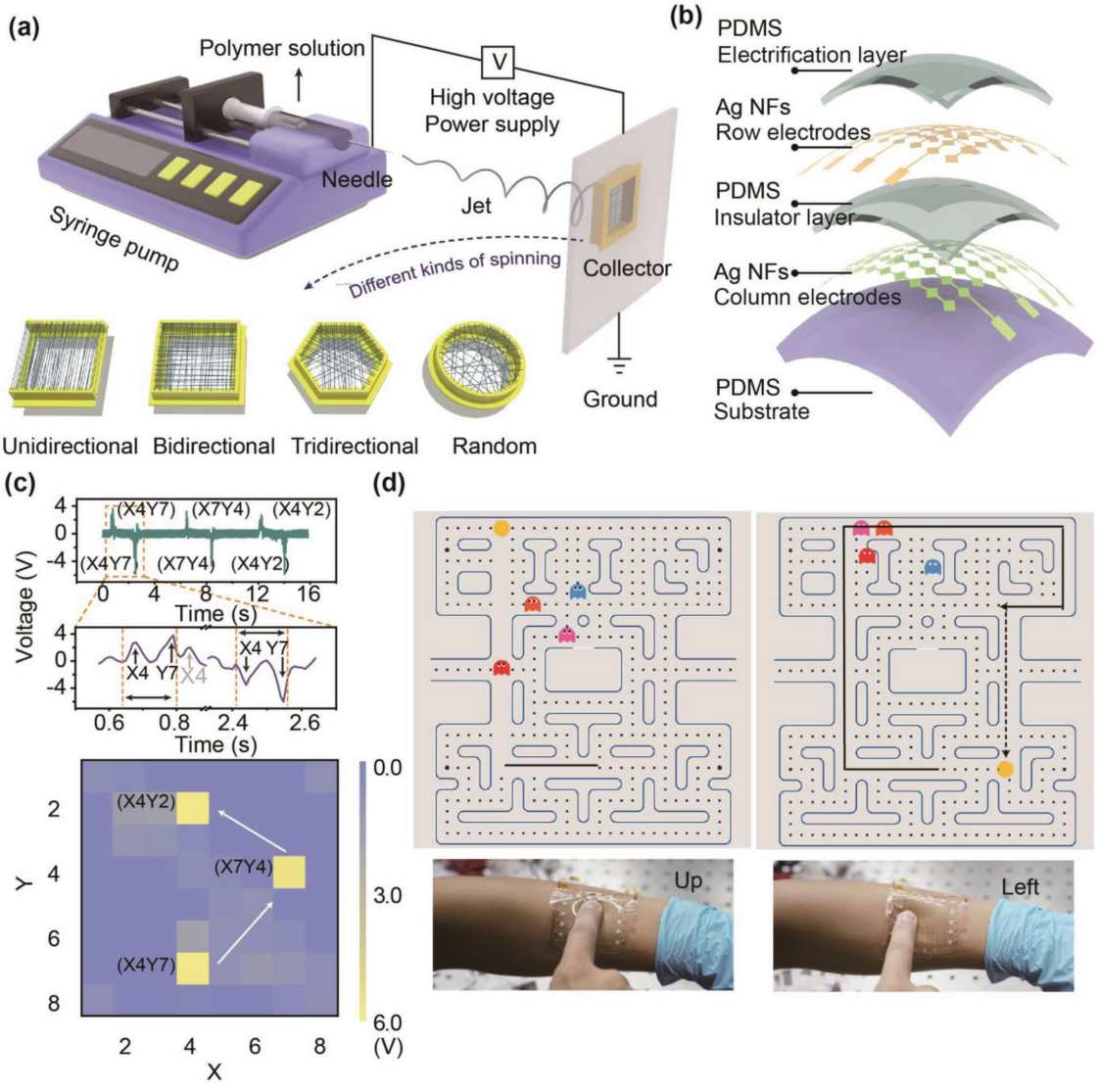

Figure 7. Highly stretchable and transparent self-powered triboelectric tactile sensor array. a) Schematic illustration of PVA NFs with different orientations by the electrospinning. b) Structure design of 8 × 8 cross-type array. c) The multiswitch scanning when the finger touched the device in sequence and the corresponding tactile mapping. d) Illustration of a Pac-Man. The pixels of the sensors are divided into four regions capable of detecting motions and different move orders will be executed when they get in touch, including moving up, down, left, and right. All panels reproduced with permission.[74] Copyright 2018, Wiley-VCH.

matrix, with the corresponding working schematic illustration depicted in Figure 8b. When applying a relative low pressure, the pressure mapping is primarily contributed by the TESM with the output voltage as a parameter for tactile imaging profile by the analysis of the software. Otherwise, under an external larger pressure, the tactile mapping will be significantly credited to the MLSM with optical signal as a valid parameter, which presents higher sensitivity than TESM due to the near saturation electric signals. Obviously, the corresponding electrical readout and optical visualization can function together to achieve a full-range pressure monitoring according to the voltage and light intensity of each pixel. Experimentally, different applied pressures have been exerted by using different sizes of contact object to accomplish an "N" shape with the route from A to D, with the corresponding mapping illustrated in Figure 8d. It can be observed that the applied pressure increases from A to C, with a reliable electrical readout of TESM in low pressure, but a distinct visible image of MLSM in high pressure. Based on the profile, the maximum light intensity occurs in the point C, illustrating

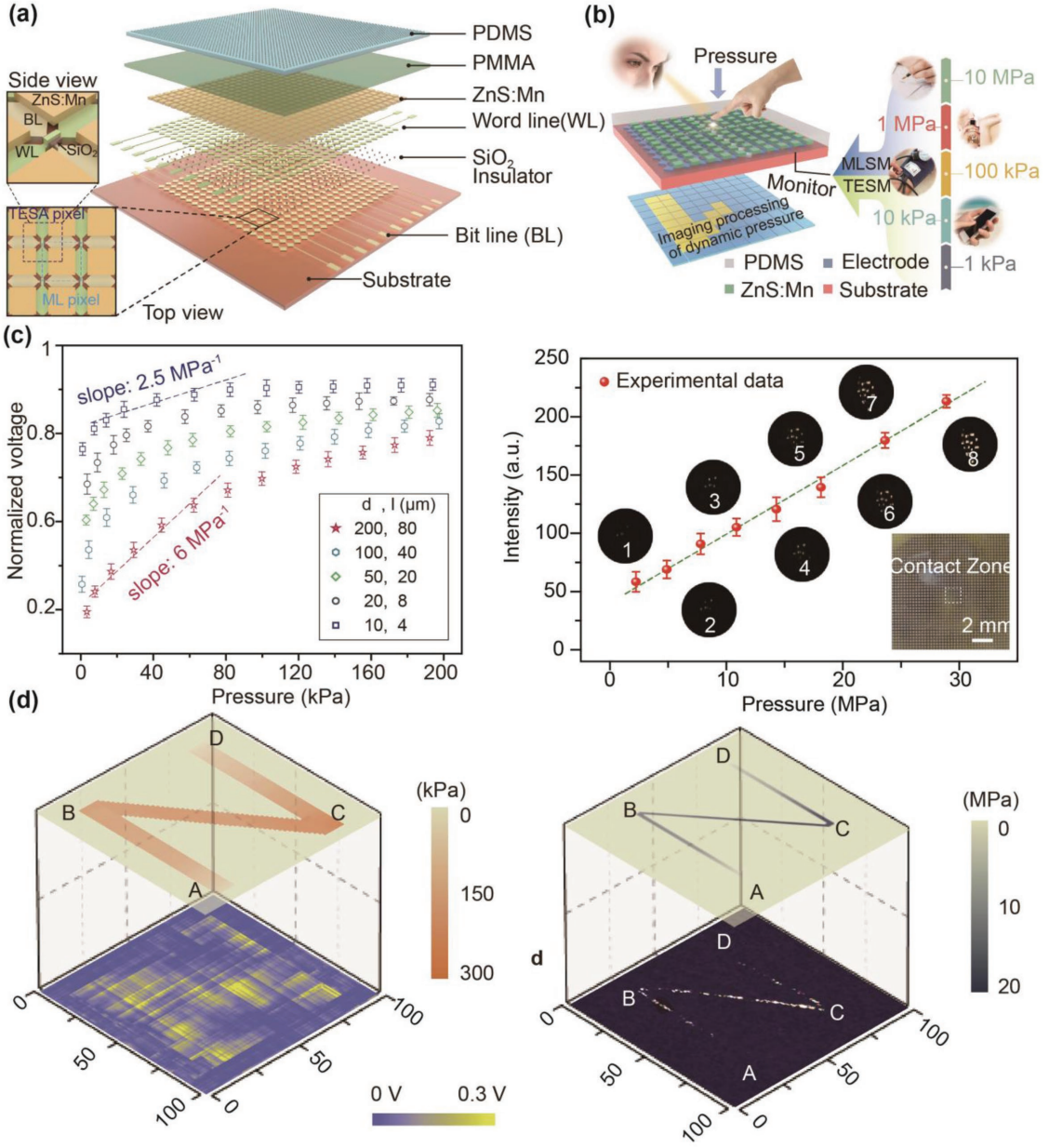

Figure 8. Full dynamic-range pressure sensor matrix based on triboelectric and mechanoluminescent sensing. a) Schematic structure of the pressure sensor matrix. b) Schematic diagram of the pressure imaging principle: TESM used for low pressure regimes (<500 kPa) and the MLSM used for high pressure regimes (>1 MPa). c) The variation of electrical and optical signals of TESM and MLSM under different applied pressures. d) Pressure mapping and electrical output voltage, and optical signal from low and high pressure regions, respectively. All panels reproduced with permission.[112] Copyright 2017, Wiley-VCH.

the validity of dual mode sensing, in accordance to the theoretical outlook initially.

Furthermore, the electrostatic potential created by the triboelectric effect can serve as a gate voltage to control or tune charge carriers transport in the channel of transistors, called tribotronic transistor (TTA),[113–115] opening up a new approach for elevating the performance since tactile sensor array based on the transistor can reduce the crosstalk sensor arrays based on transistors.[109,116,117] Herein, a typical TTA array will be focused on to explain the working mechanism, The basic unit is composed of a transistor unit and a square Cu pad, and a PTFE film is utilized to sever as the mobile triboelectric material under the external force,[113] as shown in **Figure 9**a. According to the corresponding drain–source current response of each pixel to the distance, a high sensitivity of 1.029 mm^{-1} even with a slight distance increase can be achieved (Figure 9b). Herein, the variation of distance gap between Cu pad and PTFE is represented by the difference of applied pressure. However, when the PTFE film surpasses a "critical distance" of 3 mm, a distinct sensitivity decrease can be observed. The critical distance represents when the separation distance is lower than 3 mm, the variation of output voltage in this region is larger than that of other separation distance, thus receiving a higher sensitivity. Thus, a 10×10 TTA is fabricated to demonstrate the mapping. A PTFE patch with the shape of "A" is adopted to press in the matrix, and the I_{DS} of all pixels are used for the distribution mapping (Figure 9c). The results exhibit an excellent uniformity in electrical characteristics among all 100 pixels, with 94% of the output current values in the narrow range of 0.105 ± 0.009 A, and obvious current variations can be found in contact and noncontact pixels, showing a superior performance. Additionally, a novel combination of triboelectric effect and electroluminescence (EL) is developed to visualize the pressure mapping,[118] which is fundamentally a type of triboelectrification-induced electroluminescence (TIEL) that will convert dynamic motions into luminescence to achieve visualization imaging. Different from combination of ML, the triboelectric effect plays an induced function in which the generated electric potential is used to excite the EL. A matrix is fabricated by layer-by-layer composite material employed to demonstrate real-time visualization, where the luminescent layer is prepared into a segmented structure with phosphor particles filled into the cell of one pixel to promote the spatial resolution (Figure 9d). Under an extremely low pressure less than 10 kPa, the substantial luminescence can be induced with three orders of magnitude smaller than that of elastico-triboluminescence (ETL); and the pressure sensitivity could reach 0.03 kPa^{-1} under 20 kPa, presenting a 750-fold enhancement than the ETL, with the intensity variation as a function of pressure displayed in Figure 9e. In order to achieve visualization, an image acquisition system is programed for the demonstration, as depicted in Figure 9f, where the luminescence induced by a sliding object is captured by a camcorder and a live image and the overall trajectory of the luminescence are presented in a two-window software interface. The word "light" is written to achieve the visualization of handwriting, where the separate frames will be combined and superimposed together, yielding an overall trajectory of a complete letter. Notably, the distinct variation of luminescence intensity can be observed because the applied force as well as the velocity significantly will vary during the writing. Integrated with the EL via the produced electric potential in triboelectric effect, the tactile mapping array has succeeded in realizing the visualization mapping. At the same time, a potentially high spatial resolution is available since the phosphor of finer particle size can be further promoted in segmented structure.

4. Self-Powered Tactile Sensor System Applications

Although the self-powered tactile sensor unit and array based on triboelectric effect are developed and enhanced for the fundamental ability of pressure detection and spatial mapping ability, a variety of application systems will be established, such as motion sensor, health monitoring, trajectory monitoring, and smart wireless control.[78,90,106,110,119–121] In this section, comprehensive applications newly demonstrated in recent years of human–machine interaction (HMI) and trajectory monitoring based on tactile sensor unit or matrix will be mainly focused on to introduce the self-powered tactile sensor system applications.

4.1. Applications in Human–Machine Interaction

Since the demonstration of triboelectric tactile sensors, plentiful investigations on HMI application have been demonstrated, especially concentrating on the typical examples of smart wireless control, intelligent keyboards, and actively perceived robot. Initially, the smart wireless control has already been demonstrated particularly by integrating with the human finger as a trigger as a remote switching between a triggered state and a static state.[72,85,106,122–124] Recently, triboelectric tactile sensor is employed on a pair of spectacle frames to capture eye blink motion, constructing two practical HMI systems consisting of the smart home control system and the wireless hands-free typing system,[124] as illustrated in **Figure 10**a. For establishing smart home control system, filter, amplifier, and relay signal processing circuit should be included, which contributes to translating the original voltage signal from blinking motion into the switching signal for the electrical appliances. This demonstration presents great convenience, such as hands-free for opening up a table lamp and electric fan or answering telephone, even self-care for the disabled. Furthermore, a hands-free typing system with eye blinking is further developed, in which virtual instrument software platform Lab View is respected to serve as a virtual keyboard with nine groups divided. The word "TENG" has been typed via eye blinking by a user with each signal in accordance with a certain letter. It can be observed that a distinct difference of voltage signal amplitude between voluntary and involuntary blink can easily be distinguished. In addition, another typical HMI application lies in intelligent keystroke capable of authenticating and even identifying users through their unique typing characteristics to obtain a smart security system. Previously, Chen et al., developed a self-powered intelligent keyboard between human fingers and keys,[122] which could detect and record the dynamic

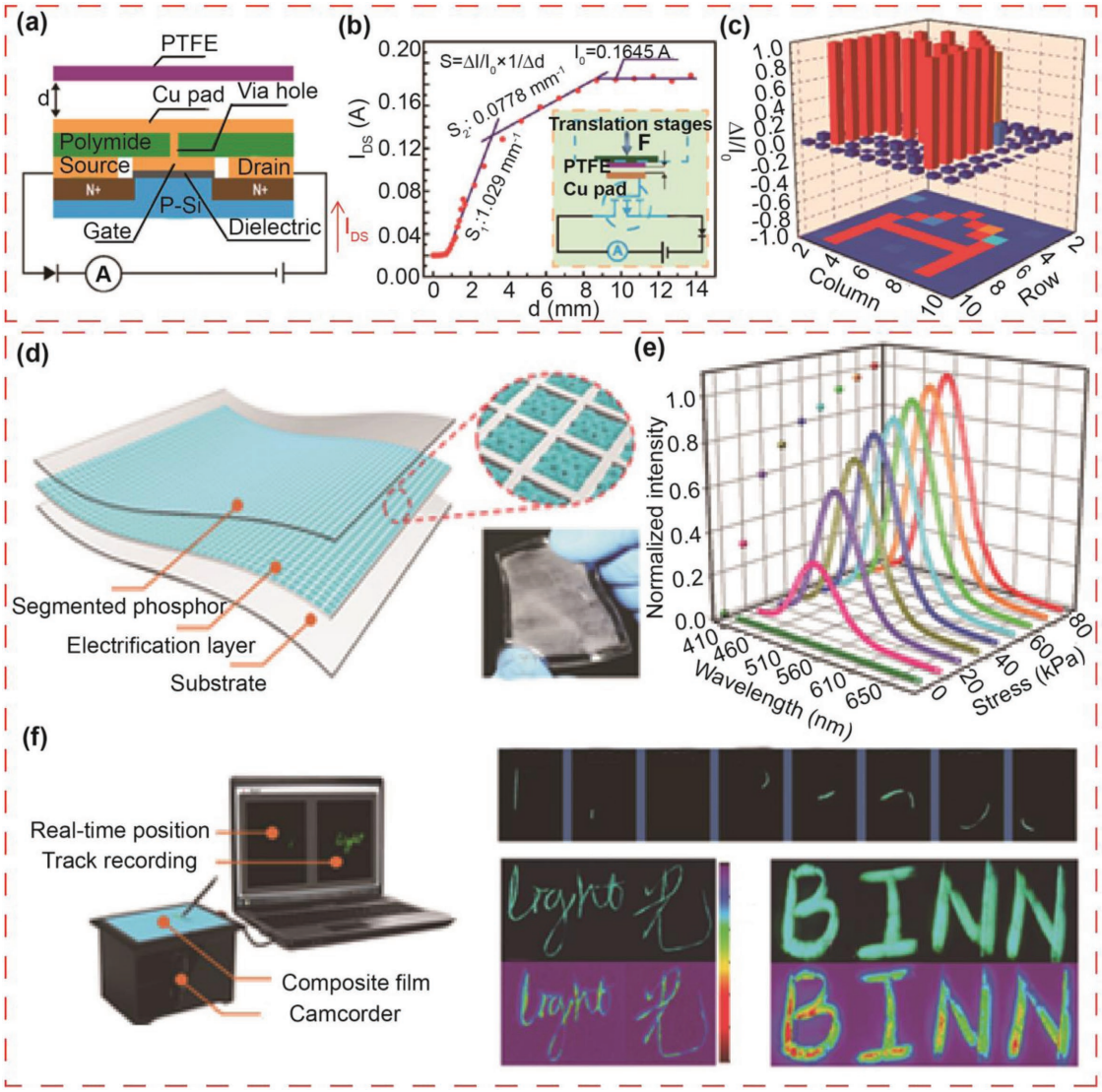

Figure 9. Tactile mapping array based on triboelectric effect integrated with transistor and electroluminescence sensing. Tribotronic transistor array for self-powered tactile sensing: a) structure schematic diagram of the basic TTA unit; b) the sensitivity curve of drain–source current response to different distance gap; c) tactile mapping in a 10 × 10 TTA matrix. Panels of a), b) and c) reproduced with permission.[113] Copyright 2016, American Chemical Society. Visualization of tactile mapping based on triboelectric-induced electroluminescence: d) structure design TIEL matrix with the segmentation structure in the luminescent layer; e) normalized intensity as a function of applied pressure; f) demonstration of image acquisition system and visualization of real-time tactile mapping depended on luminescence intensity induced by triboelectric effect. Panels of d), e) and f) reproduced with permission.[118] Copyright 2016, Wiley-VCH.

time intervals and applied pressure as typical characteristic parameter for a construction of a smart security system. Improved by the Wu et al.,[125] a two-factor authentication and identification system has been built via recording a user's intrinsic typing behavior reflected in keystroke dynamics and providing a customized signal processing scheme for feature extraction, as displayed in Figure 10b. A stretchable and conformable triboelectric keyboard consists of an improved shield electrode for minimizing the unexpected disturbing signals based on a contact–separation mode. By analyzing the characteristic parameter typing latencies (L), hold time (H), and signal magnitudes (M), the typical radar plots of the normalized average feature values have been recoded and analyzed when five users typed the same number sequence for 150 times. It can be discovered that a distinctive typing behaviors are observed among them, which provided a valid reference for the accomplishment of the authentication and identification of the users. This self-powered security supervision provided a promising approach since the password leaking and easily replicated fingerprints all have own drawbacks. Another similar work for throat-attached anti-interference capable of voice recognition also was demonstrated.[89] Recently, a highly stretchable and sensitive triboelectric quasi-skin sensor is developed,[126] which can sense the applied pressure and proximity of object with excellent stretchability to 100% strain and a superior sensitivity of 0.29 kPa^{-1} in low pressure region. Herein,

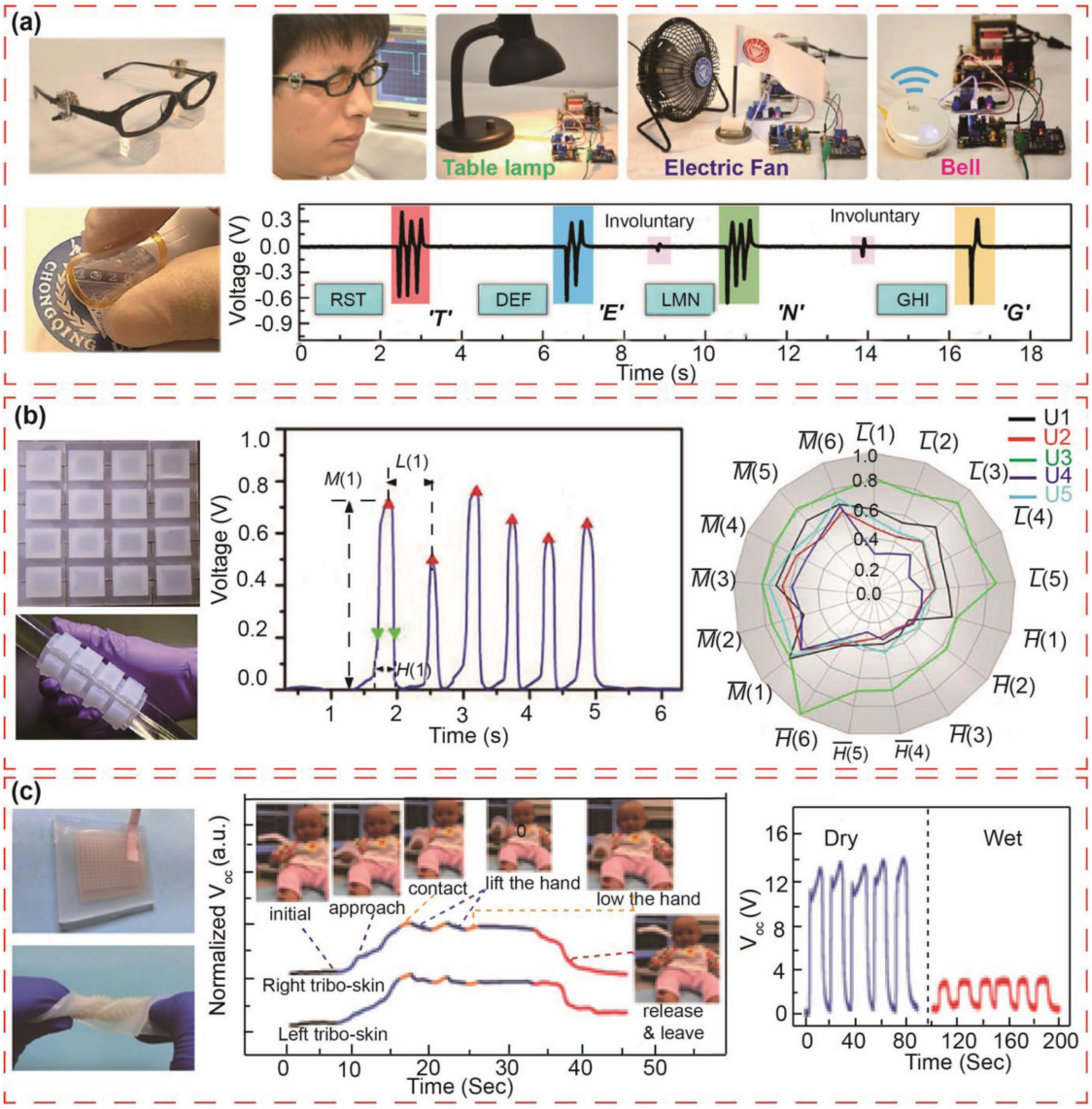

Figure 10. Human–machine interaction applications: a) application in smart home for remote wireless controlling and a hands-free typing system; Reproduced with permission.[124] Copyright 2017, American Association for the Advancement of Science; b) intelligent keystroke capable of authentication and identification; Reproduced with permission.[125] Copyright 2018, Elsevier Ltd.; c) actively perceiving and responsive soft robot hand. Reproduced with permission.[126] Copyright 2018, Wiley-VCH.

the triboelectric tactile sensors can not only sense the normal pressure, but also the proximity. In the proximity sensing mode, the object is far away from the tactile sensor originally. Once the object approaches again, the potential difference between the triboelectric sensor and object will decrease, yielding reverse electrons flowing from the ground to the embedded electrode and generating a voltage in the opposite direction. Based on this triboelectric tactile skin sensor, versatile actively perceiving and responding tasks are performed to realize the robot–human and robot–environment applications. As displayed in Figure 10c, a silicon rubber with triangular microprism structures containing Ag flake is fabricated as a stretchable and twisting active tactile sensor based on the single-electrode mode. Then, this tribo-skin is monolithically integrated onto the two fingers of the soft robots to serve as an actively perceptive and responsive soft gripper. This perceivable gripper can hold and shake a baby doll's hand with excellent adaptive compliance and superior perceived capability for unpredictable environment. It can be observed that once the gripper hand equipped with triboelectric tactile sensor approaches the doll's hand, the voltage is produced as a fast response corresponding to the proximity of the tribo-skins. When the gripper holds the baby's hand completely, the value is mounted to the maximum, in accordance to the pressure sensing of the tribo-skins. While the active gripper lifts the hand up and down, the real time–generated voltages accord with the corresponding motions, and will decrease and recover to the original value gradually under the circumstance that the gripper releases the hand. Furthermore, the designed tribo-skin can differentiate the moisture of the baby's pants to demonstrate the intelligent robots applications in interacting

with human body. Due to the reduction of triboelectric charges on the rubber surfaces in the presence of water molecules, a lower voltage signal will be detected by the wet pant than that of the dry, respectively.

4.2. Applications in Trajectory Tracking

Another significant and typical application lies in the real-time tracking of movement of a moving subject, which is the reflex of touch or non-touch state and real-time position. With respect to this practical application, Yi et al. developed triboelectric sensors to precisely detect the movement of a mobile object, in which the trajectory, velocity, and acceleration had been deduced according to the measured output signals including the open-circuit voltage and short-circuit current.[127] Many researches about trajectory monitoring have been demonstrated based on triboelectric tactile sensor arrays. Herein, several examples have been illustrated in line with the development by our group as followed. First, motion tracking system is proved to monitor moving speed, direction, acceleration, and position location.[128] As shown in **Figure 11**a, the corresponding structure design has been illustrated, where a set of triboelectric sensors are composed of fixed friction material Kapton/PMMA in different sizes with back copper electrodes and mobile triboelectric material aluminum. Due to the different sizes of each stationary Kapton, the absolute output signal value will be obtained in proportion to the contact area of each triboelectric sensor. According to the measured time interval (Δt) between two adjacent peaks, the speed can be deduced according to $v = \Delta d/\Delta t$, where Δd is the distance between two adjacent triboelectric sensors, and the acceleration can be calculated via the speed as a function of time curve. Furthermore, 8×8 (x, y) coordinates have been created to monitor the moving path by 16 triboelectric sensors with two kinds of sensors, which are composed of a long shape with high signal and a short shape with low signal, representing "1" and "0" in the binary system, respectively. Thus, a trajectory tracking of a moving path of an object can be implemented, providing potential applications in position locating, motion tracking, and even home security monitoring. Another real-time monitoring movement sensor combined with a robot's finger based on triboelectric effect has been recently demonstrated by our group,[129] as exhibited in Figure 11b. The basic unit combined with the manipulator contains two segments, in which one part FEP/Al/PET is adhered to the back of the hand acting as a stationary plate and another part Al/PET acts as contact material with an arch shape. In order to realize the movement monitoring of a finger, the triboelectric sensors with different contact areas are prepared to be attached to joints of a finger including top, middle, and bottom joint as monitoring sensors. Under the bending and unbending movements of a joint, the corresponding contact and separation processes will be accomplished, yielding different output signals according with different joints due to the unlike contact area. Furthermore, the transferred charge quantity is chosen as a characteristic parameter due to the independence on the moving operation rate. Thus, the characteristic value of the top, middle, top and middle, and bottom are ≈15, 25, 40, and 78 nC, respectively, under the entire bending and unbending operations. A real-time monitoring for a complicated and random movement of a finger has been demonstrated. According to the real time–transferred charge curve, it can be inferred that the top, middle, and bottom joints are bended in sequence according to the characteristic parameters and magnitude sequence of the various joints. Until to the highest point where the entire finger is fully bended, the middle, top, and bottom joints are successively unbended in line with the declining curve. Furthermore, on the basis of the large-scale high resolution tactile sensor array based on the single-electrode mode, a trajectory tracking capable of detecting the motion of a moving object on the surface of the matrix has been demonstrated,[73] as shown in Figure 11c. Herein, sliding mode has been involved in monitoring the path of a moving object based on the tactile sensor based on single-electrode mode. The change in effective contact area of each unit is dependent on the object's speed, leading to a change in voltage. The amplitude of the output voltage is independent on the touch frequency in the contact mode, while is significantly enhanced with the sliding speed of the object in sliding mode. Experimentally, trajectory imaging of different moving speeds of object have been profiled according to their output voltages. It can be revealed that a higher speed resulted in a higher output voltage, which will provide a better signal-to-noise ratio (SNR) of tracking mapping. When the moving speed is 10 mm s^{-1}, three voltage peaks are collected in each scanning cycle when sliding across each pixel, revealing that the change in the effective contact area per cycle occupies approximately one-third the area of the electrode in each pixel. Finally, the trajectory monitoring process will be achieved via the positive and negative voltage signals, and whole voltage signals, respectively.

5. Conclusion and Perspective

Flexible tactile sensors which possess the capability of sensing external physical stimuli have been demonstrated in various applications via conventional physical transduction mechanisms. However, some challenges remain to be settled, in which sensors cannot work independently without extra power supplier, largely hindering the practical application in flexible wearable electronics, implanted, or embedded devices. Thus, the establishment of a self-powered tactile sensor has provided an alternative to handle the puzzle, which can actively sense the stimulation without any other external power consumption. In this review, a development in self-powered tactile sensor array system based on triboelectric effect has been systematically presented from the following aspects: the fundamental mechanism of triboelectric effect, device design, development of tactile sensors unit and array, and the systematic applications (**Figure 12**). Various micro-/nanostructures of materials are decorated to enhance the performance of a tactile sensor. And, the overall trend of device design in self-powered tactile sensors based on triboelectric effect presents the combination of functionalization and high performance toward stretchable, transparent, high sensitivity, wide detect range characteristics, etc. For the tactile sensor unit, a development in performance and function two aspects is summarized based on the two primary modes including vertical contact–separation and single-electrode. For the pressure mapping array, the resolution is significantly

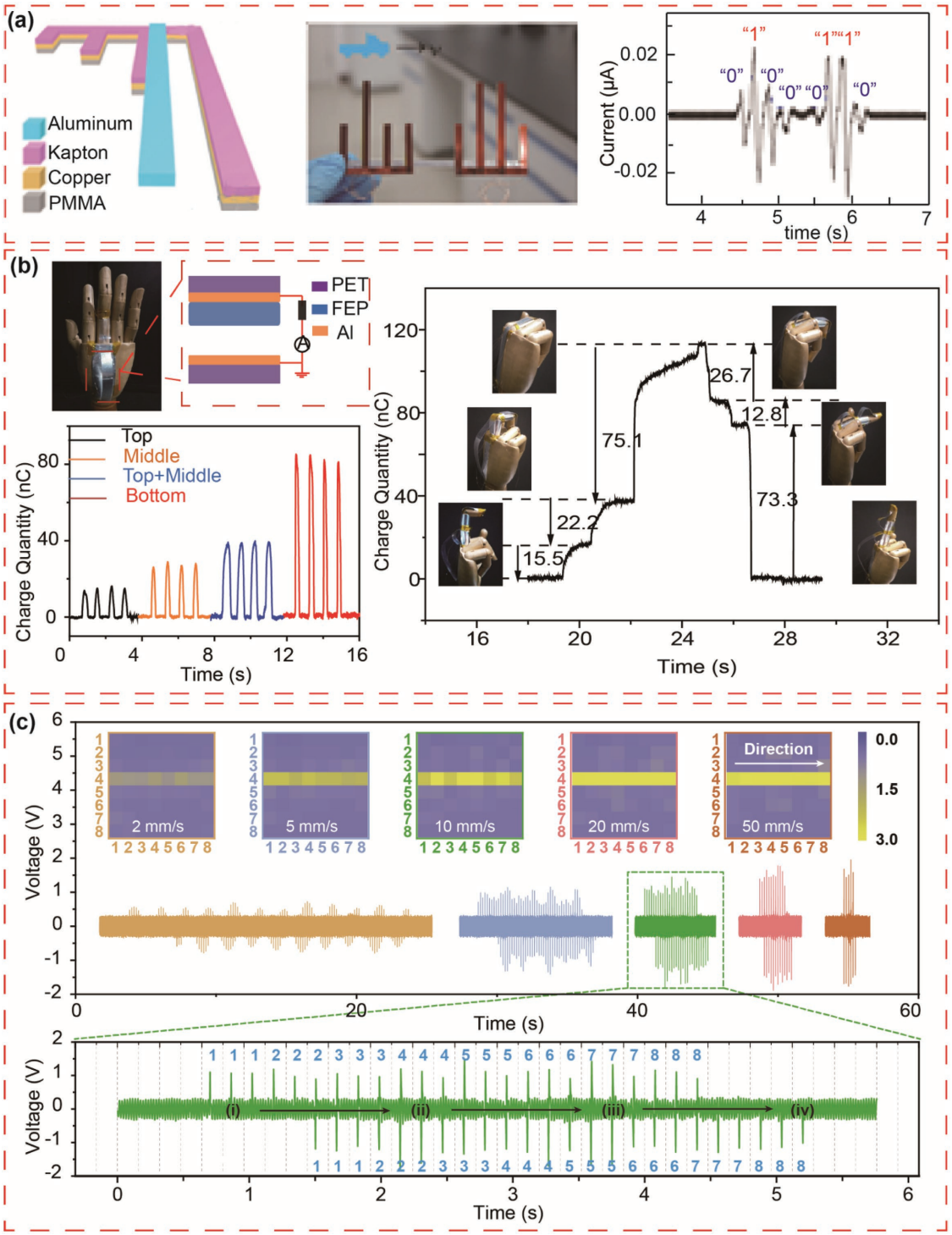

Figure 11. Applications in trajectory monitoring. a) Motion tracking system for monitoring speed, direction, acceleration, and position location. Reproduced with permission.[128] Copyright 2014, Wiley-VCH. b) Real-time movement monitoring of a finger based on different area TENG array. Reproduced under the terms and conditions of the Creative Commons Attribution 4.0 International License.[129] Copyright 2017, The Authors, published by Springer Nature. c) Real-time trajectory imaging of different speeds of moving objects on the 8 × 8 array. Reproduced with permission.[73] Copyright 2016, Wiley-VCH.

enhanced by the novel cross-type configuration based on single-electrode mode, with the corresponding scanning channels reduced. Integrated with mechanoluminescence and electroluminescence, the broadening of detect range and visualization of pressure imaging are achieved, while the integration with transistor will provide a potential approach for implementing high performance of self-powered tactile sensor system. Finally systematic applications are demonstrated in various aspects,

where two main aspects of human–machine interface and trajectory monitoring will be systematically summarized.

Despite of significant enhancements in self-powered tactile sensor system based on triboelectric effect have been demonstrated, certain challenges remain. 1) A triboelectric tactile sensor will be respected to present not only high basic performance such as high sensitivity and resolution, wide detect range, fast response, and good linearity, but also multifunction including stretchable, transparent, even compliant and self-healing properties, because those properties are necessary elements for complicated practical applications in robots, human–machine interface, and biomedicine. Thus, the micro-/nanostructure of contact surface, hierarchical structure of devices, and novel materials and structure design should be further developed and integrated to achieve the superior comprehensive performance. 2) Apart from the constructing of self-powered system, integrated with other transduction mechanisms, versatile and heterogeneous sensing capabilities for pressure, strain, touch, temperature, and humidity should be embodied in an integrated tactile unit or matrix not just a monosensing ability, mimicking the human skin for perceiving of multiple stimuli in a complicated environment. 3) Additionally, when a higher spatial resolution has been promoted, the corresponding output electric signals will be minimized responsively due to the reduction of effective contact area, which will prevent the feasibility of measurement process due to the bad SNR resulting from the tiny and weak signals. Thus, further improvement on pressure mapping resolution may be achieved by integrating with other mechanisms such as transistor or adopting more novel and optimal integration methods.

Acknowledgements

J.T. and R.B. contributed equally to this work. The authors express thanks for the support from the National Key R & D Project from the Minister of Science and Technology, China (Grant No. 2016YFA0202703), the National Natural Science Foundation of China (Grant Nos. 51622205, 61675027, 51432005, 61505010, and 51502018), the Beijing Council of Science and Technology (Grant Nos. Z171100002017019 and Z181100004418004), the Natural Science Foundation of Beijing Municipality (Grant Nos. 4181004, 4182080, 4184110, and 2184131),

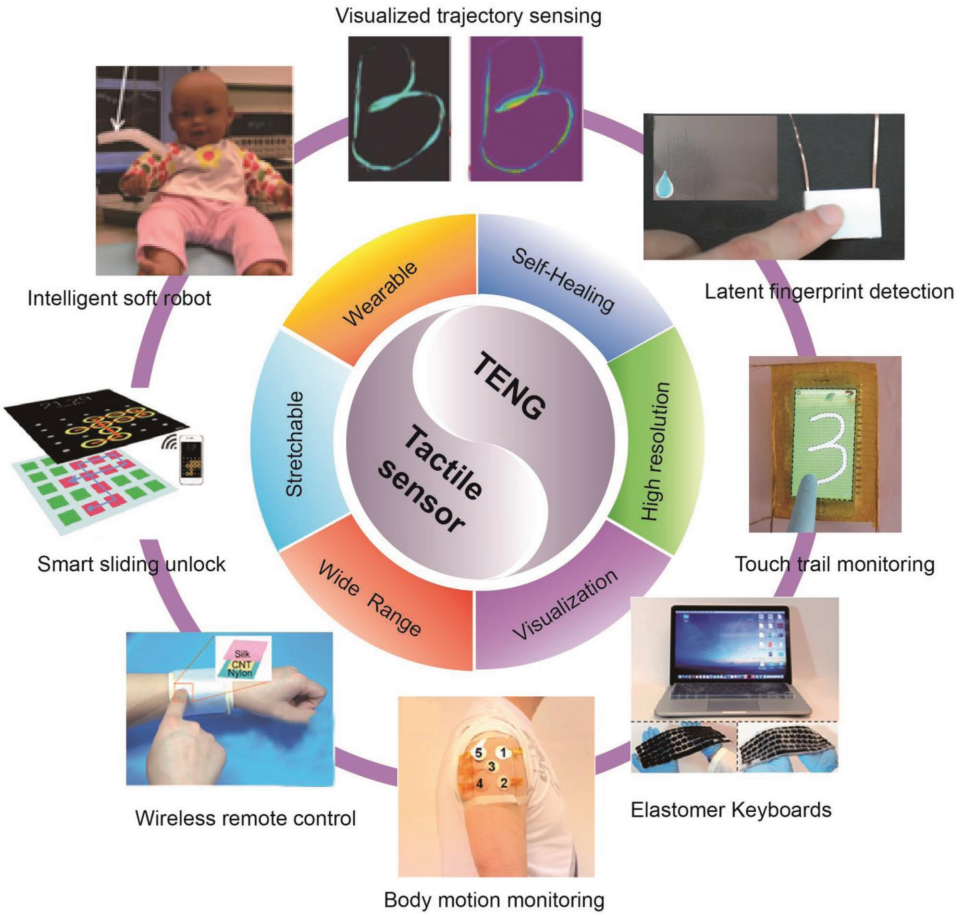

Figure 12. Diagram of self-powered tactile sensor based on triboelectric effect and applications: body motion monitoring. Reproduced with permission.[120] Copyright 2014, American Chemical Society; wireless remote controlling. Reproduced with permission.[106] Copyright 2018, American Chemical Society; smart sliding unlock. Reproduced with permission.[110] Copyright 2017, American Chemical Society; intelligent soft robot. Reproduced with permission.[126] Copyright 2018, Wiley-VCH; visualized trajectory sensing.[118] Copyright 2016, Wiley-VCH; latent fingerprint detection. Reproduced with permission.[121] Copyright 2016, American Chemical Society; touch trail monitoring. Reproduced with permission.[73] Copyright 2016, Wiley-VCH; elastomer keyboards. Reproduced with permission.[123] Copyright 2016, American Chemical Society.

and the "Thousand Talents" Program of China for pioneering researchers and innovative teams.

Conflict of Interest

The authors declare no conflict of interest.

Keywords

self-powered systems, tactile sensors, triboelectric effect

Received: September 9, 2018
Revised: October 15, 2018
Published online:

[1] A. Chortos, J. Liu, Z. Bao, *Nat. Mater.* **2016**, *15*, 937.
[2] T. T. Yang, D. Xie, Z. H. Li, H. W. Zhu, *Mater. Sci. Eng., R* **2017**, *115*, 1.
[3] Y. Wan, Y. Wang, C. F. Guo, *Mater. Today Phys.* **2017**, *1*, 61.
[4] M. L. Hammock, A. Chortos, B. C.-K. Tee, J. B.-H. Tok, Z. Bao, *Adv. Mater.* **2013**, *25*, 5997.
[5] Y. Ma, N. Liu, L. Li, X. Hu, Z. Zou, J. Wang, S. Luo, Y. Gao, *Nat. Commun.* **2017**, *8*, 1207.
[6] J. Park, Y. Lee, J. Hong, M. Ha, Y.-D. Jung, H. Lim, S. Y. Kim, H. Ko, *ACS Nano* **2014**, *8*, 4689.
[7] Q. Hua, H. Liu, J. Zhao, D. Peng, X. Yang, L. Gu, C. Pan, *Adv. Electron. Mater.* **2016**, *2*, 1600093.
[8] S. Gong, W. Schwalb, Y. Wang, Y. Chen, Y. Tang, J. Si, B. Shirinzadeh, W. Cheng, *Nat. Commun.* **2014**, *5*, 2132.
[9] C. Wang, J. Zhao, C. Ma, J. Sun, L. Tian, X. Li, F. Li, X. Han, C. Liu, C. Shen, L. Dong, J. Yang, C. Pan, *Nano Energy* **2017**, *34*, 578.
[10] L. W. Yap, S. Gong, Y. Tang, Y. Zhu, W. Cheng, *Sci. Bull.* **2016**, *61*, 1624.
[11] X. Zhao, Q. Hua, R. Yu, Y. Zhang, C. Pan, *Adv. Electron. Mater.* **2015**, *1*, 1500142.
[12] D. P. J. Cotton, I. M. Graz, S. P. Lacour, *IEEE Sens. J.* **2009**, *9*, 2008.
[13] S. C. B. Mannsfeld, B. C. K. Tee, R. M. Stoltenberg, C. V. H. H. Chen, S. Barman, B. V. O. Muir, A. N. Sokolov, C. Reese, Z. Bao, *Nat. Mater.* **2010**, *9*, 859.
[14] B. Nie, R. Li, J. Cao, J. D. Brandt, T. Pan, *Adv. Mater.* **2015**, *27*, 6055.
[15] M. Ramuz, B. C.-K. Tee, J. B.-H. Tok, Z. Bao, *Adv. Mater.* **2012**, *24*, 3223.
[16] H.-H. Chou, A. Nguyen, A. Chortos, J. W. F. To, C. Lu, J. Mei, T. Kurosawa, W.-G. Bae, J. B.-H. Tok, Z. Bao, *Nat. Commun.* **2015**, *6*, 8011.
[17] D. Son, J. Lee, S. Qiao, R. Ghaffari, J. Kim, J. E. Lee, C. Song, S. J. Kim, D. J. Lee, S. W. Jun, S. Yang, M. Park, J. Shin, K. Do, M. Lee, K. Kang, C. S. Hwang, N. Lu, T. Hyeon, D.-H. Kim, *Nat. Nanotechnol.* **2014**, *9*, 397.
[18] Y.-L. Xu, X.-H. Zhang, S. Zhu, S. Zhan, *Sci. Bull.* **2016**, *61*, 313.
[19] M. Ha, S. Lim, H. Ko, *J. Mater. Chem. B* **2018**, *6*, 4043.
[20] Q. Hua, J. Sun, H. Liu, R. Bao, R. Yu, J. Zhai, C. Pan, Z. L. Wang, *Nat. Commun.* **2018**, *9*, 244.
[21] Z. Lou, L. Li, L. Wang, G. Shen, *Small* **2017**, *13*, 1701791.
[22] S. Wang, L. Lin, Z. L. Wang, *Nano Energy* **2015**, *11*, 436.
[23] Z. Wen, Q. Shen, X. Sun, *Nano-Micro Lett.* **2017**, *9*, 45.
[24] G. Zhu, B. Peng, J. Chen, Q. Jing, Z. Lin Wang, *Nano Energy* **2015**, *14*, 126.
[25] X. Cao, Y. Jie, N. Wang, Z. L. Wang, *Adv. Energy Mater.* **2016**, *6*, 1600665.
[26] M. Law, L. E. Greene, J. C. Johnson, R. Saykally, P. Yang, *Nat. Mater.* **2005**, *4*, 455.
[27] W. Ma, C. Yang, X. Gong, K. Lee, A. J. Heeger, *Adv. Funct. Mater.* **2005**, *15*, 1617.
[28] W. Guo, X. Zhang, R. Yu, M. Que, Z. Zhang, Z. Wang, Q. Hua, C. Wang, Z. L. Wang, C. Pan, *Adv. Energy Mater.* **2015**, *5*, 1500141.
[29] G. Hu, W. Guo, R. Yu, X. Yang, R. Zhou, C. Pan, Z. L. Wang, *Nano Energy* **2016**, *23*, 27.
[30] T. J. Kang, S. Fang, M. E. Kozlov, C. S. Haines, N. Li, Y. H. Kim, Y. Chen, R. H. Baughman, *Adv. Funct. Mater.* **2012**, *22*, 477.
[31] H. Im, T. Kim, H. Song, J. Choi, J. S. Park, R. Ovalle-Robles, H. D. Yang, K. D. Kihm, R. H. Baughman, H. H. Lee, T. J. Kang, Y. H. Kim, *Nat. Commun.* **2016**, *7*, 10600.
[32] F. R. Fan, W. Tang, Z. L. Wang, *Adv. Mater.* **2016**, *28*, 4283.
[33] X. He, Y. Zi, H. Yu, S. L. Zhang, J. Wang, W. Ding, H. Zou, W. Zhang, C. Lu, Z. L. Wang, *Nano Energy* **2017**, *39*, 328.
[34] Q. Jing, Y. Xie, G. Zhu, R. P. S. Han, Z. L. Wang, *Nat. Commun.* **2015**, *6*, 8031.
[35] Z. L. Wang, J. Chen, L. Lin, *Energy Environ. Sci.* **2015**, *8*, 2250.
[36] Z. L. Wang, G. Zhu, Y. Yang, S. Wang, C. Pan, *Mater. Today* **2012**, *15*, 532.
[37] J. Sun, X. Pu, C. Jiang, C. Du, M. Liu, Y. Zhang, Z. Liu, J. Zhai, W. Hu, Z. L. Wang, *Sci. Bull.* **2018**, *63*, 795.
[38] W. Du, X. Han, L. Lin, M. Chen, X. Li, C. Pan, Z. L. Wang, *Adv. Energy Mater.* **2014**, *4*, 1301592.
[39] Q. Zhang, T. Jiang, D. Ho, S. Qin, X. Yang, J. H. Cho, Q. Sun, Z. L. Wang, *ACS Nano* **2018**, *12*, 254.
[40] Z. L. Wang, *Faraday Discuss.* **2014**, *176*, 447.
[41] C. Deng, W. Tang, L. Liu, B. Chen, M. Li, Z. L. Wang, *Adv. Funct. Mater.* **2018**, *28*, 1801606.
[42] Z. L. Wang, J. Song, *Science* **2006**, *312*, 242.
[43] C. Pan, L. Dong, G. Zhu, S. Niu, R. Yu, Q. Yang, Y. Liu, Z. L. Wang, *Nat. Photonics* **2013**, *7*, 752.
[44] R. Bao, C. Wang, L. Dong, C. Shen, K. Zhao, C. Pan, *Nanoscale* **2016**, *8*, 8078.
[45] R. Bao, C. Wang, L. Dong, R. Yu, K. Zhao, Z. L. Wang, C. Pan, *Adv. Funct. Mater.* **2015**, *25*, 2884.
[46] X. Wang, H. Zhang, R. Yu, L. Dong, D. Peng, A. Zhang, Y. Zhang, H. Liu, C. Pan, Z. L. Wang, *Adv. Mater.* **2015**, *27*, 2324.
[47] C. Wang, R. Bao, K. Zhao, T. Zhang, L. Dong, C. Pan, *Nano Energy* **2015**, *14*, 364.
[48] C. Pan, M. Chen, R. Yu, Q. Yang, Y. Hu, Y. Zhang, Z. L. Wang, *Adv. Mater.* **2016**, *28*, 1535.
[49] F. R. Fan, Z. Q. Tian, Z. L. Wang, *Nano Energy* **2012**, *1*, 328.
[50] F. Yi, L. Lin, S. Niu, P. K. Yang, Z. Wang, J. Chen, Y. Zhou, Y. Zi, J. Wang, Q. Liao, Y. Zhang, Z. L. Wang, *Adv. Funct. Mater.* **2015**, *25*, 3688.
[51] L. Zhang, B. Zhang, J. Chen, L. Jin, W. Deng, J. Tang, H. Zhang, H. Pan, M. Zhu, W. Yang, Z. L. Wang, *Adv. Mater.* **2016**, *28*, 1650.
[52] X. Li, J. Tao, W. Guo, X. Zhang, J. Luo, M. Chen, J. Zhu, C. Pan, *J. Mater. Chem. A* **2015**, *3*, 22663.
[53] X. Li, J. Tao, X. Wang, J. Zhu, C. Pan, Z. L. Wang, *Adv. Energy Mater.* **2018**, *8*, 1800705.
[54] Y. Xi, H. Guo, Y. Zi, X. Li, J. Wang, J. Deng, S. Li, C. Hu, X. Cao, Z. L. Wang, *Adv. Energy Mater.* **2017**, *7*, 1602397.
[55] Z.-H. Lin, G. Cheng, X. Li, P.-K. Yang, X. Wen, Z. L. Wang, *Nano Energy* **2015**, *15*, 256.
[56] C. Wu, R. Liu, J. Wang, Y. Zi, L. Lin, Z. L. Wang, *Nano Energy* **2017**, *32*, 287.
[57] M. Xu, P. Wang, Y.-C. Wang, S. L. Zhang, A. C. Wang, C. Zhang, Z. Wang, X. Pan, Z. L. Wang, *Adv. Energy Mater.* **2018**, *8*, 1702432.
[58] M. Ha, J. Park, Y. Lee, H. Ko, *ACS Nano* **2015**, *9*, 3421.
[59] Y. Ma, Q. Zheng, Y. Liu, B. Shi, X. Xue, W. Ji, Z. Liu, Y. Jin, Y. Zou, Z. An, W. Zhang, X. Wang, W. Jiang, Z. Xu, Z. L. Wang, Z. Li, H. Zhang, *Nano Lett.* **2016**, *16*, 6042.

[60] H. Guo, X. Pu, J. Chen, Y. Meng, M.-H. Yeh, G. Liu, Q. Tang, B. Chen, D. Liu, S. Qi, C. Wu, C. Hu, J. Wang, Z. L. Wang, *Sci. Rob.* **2018**, *3*, eaat2516.
[61] Z. Ren, J. Nie, J. Shao, Q. Lai, L. Wang, J. Chen, X. Chen, Z. L. Wang, *Adv. Funct. Mater.* **2018**, *28*, 1802989.
[62] Z. L. Wang, *ACS Nano* **2013**, *7*, 9533.
[63] J. Chen, Z. L. Wang, *Joule* **2017**, *1*, 480.
[64] Z. L. Wang, *Mater. Today* **2017**, *20*, 74.
[65] C. Xu, Y. Zi, A. C. Wang, H. Zou, Y. Dai, X. He, P. Wang, Y.-C. Wang, P. Feng, D. Li, Z. L. Wang, *Adv. Mater.* **2018**, *30*, 1706790.
[66] L. S. McCarty, A. Winkleman, G. M. Whitesides, *J. Am. Chem. Soc.* **2007**, *129*, 4075.
[67] L. S. McCarty, G. M. Whitesides, *Angew. Chem., Int. Ed.* **2008**, *47*, 2188.
[68] W. R. Harper, *Proc. R. Soc. London, Ser. A* **1951**, *205*, 83.
[69] Y. S. Zhou, S. Wang, Y. Yang, G. Zhu, S. Niu, Z.-H. Lin, Y. Liu, Z. L. Wang, *Nano Lett.* **2014**, *14*, 1567.
[70] C. X. Lu, C. B. Han, G. Q. Gu, J. Chen, Z. W. Yang, T. Jiang, C. He, Z. L. Wang, *Adv. Eng. Mater.* **2017**, *19*, 1700275.
[71] Z. Lin, J. Yang, X. Li, Y. Wu, W. Wei, J. Liu, J. Chen, J. Yang, *Adv. Funct. Mater.* **2018**, *28*, 1704112.
[72] P. Bai, G. Zhu, Q. Jing, J. Yang, J. Chen, Y. Su, J. Ma, G. Zhang, Z. L. Wang, *Adv. Funct. Mater.* **2014**, *24*, 5807.
[73] X. Wang, H. Zhang, L. Dong, X. Han, W. Du, J. Zhai, C. Pan, Z. L. Wang, *Adv. Mater.* **2016**, *28*, 2896.
[74] X. Wang, Y. Zhang, X. Zhang, Z. Huo, X. Li, M. Que, Z. Peng, H. Wang, C. Pan, *Adv. Mater.* **2018**, *30*, 1706738.
[75] R. Liu, X. Kuang, J. Deng, Y.-C. Wang, A. C. Wang, W. Ding, Y.-C. Lai, J. Chen, P. Wang, Z. Lin, H. J. Qi, B. Sun, Z. L. Wang, *Adv. Mater.* **2018**, *30*, 1705195.
[76] X. Chen, Y. Wu, J. Shao, T. Jiang, A. Yu, L. Xu, Z. L. Wang, *Small* **2017**, *13*, 1702929.
[77] L. Lin, Y. Xie, S. Wang, W. Wu, S. Niu, X. Wen, Z. L. Wang, *ACS Nano* **2013**, *7*, 8266.
[78] M. Ha, S. Lim, S. Cho, Y. Lee, S. Na, C. Baig, H. Ko, *ACS Nano* **2018**, *12*, 3964.
[79] X.-Z. Jiang, Y.-J. Sun, Z. Fan, T.-Y. Zhang, *ACS Nano* **2016**, *10*, 7696.
[80] J. Deng, X. Kuang, R. Liu, W. Ding, A. C. Wang, Y.-C. Lai, K. Dong, Z. Wen, Y. Wang, L. Wang, H. J. Qi, T. Zhang, Z. L. Wang, *Adv. Mater.* **2018**, *30*, 1705918.
[81] X. Pu, M. Liu, X. Chen, J. Sun, C. Du, Y. Zhang, J. Zhai, W. Hu, Z. L. Wang, *Sci. Adv.* **2017**, *3*, e1700015.
[82] Q. Zheng, Y. Zou, Y. Zhang, Z. Liu, B. Shi, X. Wang, Y. Jin, H. Ouyang, Z. Li, Z. L. Wang, *Sci. Adv.* **2016**, *2*, e1501478.
[83] F. Yi, X. Wang, S. Niu, S. Li, Y. Yin, K. Dai, G. Zhang, L. Lin, Z. Wen, H. Guo, J. Wang, M.-H. Yeh, Y. Zi, Q. Liao, Z. You, Y. Zhang, Z. L. Wang, *Sci. Adv.* **2016**, *2*, e1501624.
[84] J. Wang, C. Wu, Y. Dai, Z. Zhao, A. Wang, T. Zhang, Z. L. Wang, *Nat. Commun.* **2017**, *8*, 88.
[85] G. Zhu, W. Q. Yang, T. Zhang, Q. Jing, J. Chen, Y. S. Zhou, P. Bai, Z. L. Wang, *Nano Lett.* **2014**, *14*, 3208.
[86] P. Bai, G. Zhu, Z.-H. Lin, Q. Jing, J. Chen, G. Zhang, J. Ma, Z. L. Wang, *ACS Nano* **2013**, *7*, 3713.
[87] J. Chen, J. Yang, H. Guo, Z. Li, L. Zheng, Y. Su, Z. Wen, X. Fan, Z. L. Wang, *ACS Nano* **2015**, *9*, 12334.
[88] G. Zhu, J. Chen, Y. Liu, P. Bai, Y. S. Zhou, Q. Jing, C. Pan, Z. L. Wang, *Nano Lett.* **2013**, *13*, 2282.
[89] J. Yang, J. Chen, Y. Su, Q. Jing, Z. Li, F. Yi, X. Wen, Z. Wang, Z. L. Wang, *Adv. Mater.* **2015**, *27*, 1316.
[90] F. R. Fan, L. Lin, G. Zhu, W. Wu, R. Zhang, Z. L. Wang, *Nano Lett.* **2012**, *12*, 3109.
[91] S. Wang, L. Lin, Z. L. Wang, *Nano Lett.* **2012**, *12*, 6339.
[92] J. Wang, S. Li, F. Yi, Y. Zi, J. Lin, X. Wang, Y. Xu, Z. L. Wang, *Nat. Commun.* **2016**, *7*, 12744.
[93] F. Yi, J. Wang, X. Wang, S. Niu, S. Li, Q. Liao, Y. Xu, Z. You, Y. Zhang, Z. L. Wang, *ACS Nano* **2016**, *10*, 6519.
[94] T. Liu, M. Liu, S. Dou, J. Sun, Z. Cong, C. Jiang, C. Du, X. Pu, W. Hu, Z. L. Wang, *ACS Nano* **2018**, *12*, 2818.
[95] P.-K. Yang, L. Lin, F. Yi, X. Li, K. C. Pradel, Y. Zi, C.-I. Wu, J.-H. He, Y. Zhang, Z. L. Wang, *Adv. Mater.* **2015**, *27*, 3817.
[96] P.-K. Yang, Z.-H. Lin, K. C. Pradel, L. Lin, X. Li, X. Wen, J.-H. He, Z. L. Wang, *ACS Nano* **2015**, *9*, 901.
[97] Z. Wen, M.-H. Yeh, H. Guo, J. Wang, Y. Zi, W. Xu, J. Deng, L. Zhu, X. Wang, C. Hu, L. Zhu, X. Sun, Z. L. Wang, *Sci. Adv.* **2016**, *2*, e1600097.
[98] X. Pu, W. Song, M. Liu, C. Sun, C. Du, C. Jiang, X. Huang, D. Zou, W. Hu, Z. L. Wang, *Adv. Energy Mater.* **2016**, *6*, 1601048.
[99] X. Pu, L. Li, H. Song, C. Du, Z. Zhao, C. Jiang, G. Cao, W. Hu, Z. L. Wang, *Adv. Mater.* **2015**, *27*, 2472.
[100] K. Dong, J. Deng, Y. Zi, Y.-C. Wang, C. Xu, H. Zou, W. Ding, Y. Dai, B. Gu, B. Sun, Z. L. Wang, *Adv. Mater.* **2017**, *29*, 1702648.
[101] X. X. Zhu, X. S. Meng, S. Y. Kuang, X. D. Wang, C. F. Pan, G. Zhu, Z. L. Wang, *Nano Energy* **2017**, *41*, 387.
[102] J. Sun, X. Pu, M. Liu, A. Yu, C. Du, J. Zhai, W. Hu, Z. L. Wang, *ACS Nano* **2018**, *12*, 6147.
[103] M. S. Rasel, P. Maharjan, M. Salauddin, M. T. Rahman, H. O. Cho, J. W. Kim, J. Y. Park, *Nano Energy* **2018**, *49*, 603.
[104] Y. Yang, H. Zhang, X. Zhong, F. Yi, R. Yu, Y. Zhang, Z. L. Wang, *ACS Appl. Mater. Interfaces* **2014**, *6*, 3680.
[105] Y. Yang, H. Zhang, Z.-H. Lin, Y. S. Zhou, Q. Jing, Y. Su, J. Yang, J. Chen, C. Hu, Z. L. Wang, *ACS Nano* **2013**, *7*, 9213.
[106] R. Cao, X. Pu, X. Du, W. Yang, J. Wang, H. Guo, S. Zhao, Z. Yuan, C. Zhang, C. Li, Z. L. Wang, *ACS Nano* **2018**, *12*, 5190.
[107] H. Guo, T. Li, X. Cao, J. Xiong, Y. Jie, M. Willander, X. Cao, N. Wang, Z. L. Wang, *ACS Nano* **2017**, *11*, 856.
[108] S. W. Chen, X. Cao, N. Wang, L. Ma, H. R. Zhu, M. Willander, Y. Jie, Z. L. Wang, *Adv. Energy Mater.* **2017**, *7*, 1601255.
[109] X. Wang, L. Dong, H. Zhang, R. Yu, C. Pan, Z. L. Wang, *Adv. Sci.* **2015**, *2*, 1500169.
[110] Z. Yuan, T. Zhou, Y. Yin, R. Cao, C. Li, Z. L. Wang, *ACS Nano* **2017**, *11*, 8364.
[111] M. Ma, Z. Zhang, Q. Liao, F. Yi, L. Han, G. Zhang, S. Liu, X. Liao, Y. Zhang, *Nano Energy* **2017**, *32*, 389.
[112] X. Wang, M. Que, M. Chen, X. Han, X. Li, C. Pan, Z. L. Wang, *Adv. Mater.* **2017**, *29*, 1605817.
[113] Z. W. Yang, Y. Pang, L. Zhang, C. Lu, J. Chen, T. Zhou, C. Zhang, Z. L. Wang, *ACS Nano* **2016**, *10*, 10912.
[114] G. Gao, B. Wan, X. Liu, Q. Sun, X. Yang, L. Wang, C. Pan, Z. L. Wang, *Adv. Mater.* **2018**, *30*, 1705088.
[115] F. Xue, L. Chen, L. Wang, Y. Pang, J. Chen, C. Zhang, Z. L. Wang, *Adv. Funct. Mater.* **2016**, *26*, 2104.
[116] S. Y. Hong, Y. H. Lee, H. Park, S. W. Jin, Y. R. Jeong, J. Yun, I. You, G. Zi, J. S. Ha, *Adv. Mater.* **2016**, *28*, 930.
[117] S. Wang, J. Xu, W. Wang, G.-J. N. Wang, R. Rastak, F. Molina-Lopez, J. W. Chung, S. Niu, V. R. Feig, J. Lopez, T. Lei, S.-K. Kwon, Y. Kim, A. M. Foudeh, A. Ehrlich, A. Gasperini, Y. Yun, B. Murmann, J. B. H. Tok, Z. Bao, *Nature* **2018**, *555*, 83.
[118] X. Y. Wei, X. Wang, S. Y. Kuang, L. Su, H. Y. Li, Y. Wang, C. Pan, Z. L. Wang, G. Zhu, *Adv. Mater.* **2016**, *28*, 6656.
[119] C. Bao Han, C. Zhang, X. H. Li, L. Zhang, T. Zhou, W. Hu, Z. Lin Wang, *Nano Energy* **2014**, *9*, 325.
[120] W. Yang, J. Chen, X. Wen, Q. Jing, J. Yang, Y. Su, G. Zhu, W. Wu, Z. L. Wang, *ACS Appl. Mater. Interfaces* **2014**, *6*, 7479.
[121] Y. Jie, H. Zhu, X. Cao, Y. Zhang, N. Wang, L. Zhang, Z. L. Wang, *ACS Nano* **2016**, *10*, 10366.
[122] J. Chen, G. Zhu, J. Yang, Q. Jing, P. Bai, W. Yang, X. Qi, Y. Su, Z. L. Wang, *ACS Nano* **2015**, *9*, 105.
[123] S. Li, W. Peng, J. Wang, L. Lin, Y. Zi, G. Zhang, Z. L. Wang, *ACS Nano* **2016**, *10*, 7973.

[124] X. Pu, H. Guo, J. Chen, X. Wang, Y. Xi, C. Hu, Z. L. Wang, *Sci. Adv.* **2017**, *3*, e1700694.
[125] C. Wu, W. Ding, R. Liu, J. Wang, A. C. Wang, J. Wang, S. Li, Y. Zi, Z. L. Wang, *Mater. Today* **2018**, *21*, 216.
[126] Y.-C. Lai, J. Deng, R. Liu, Y.-C. Hsiao, S. L. Zhang, W. Peng, H.-M. Wu, X. Wang, Z. L. Wang, *Adv. Mater.* **2018**, *30*, 1801114.
[127] F. Yi, L. Lin, S. Niu, J. Yang, W. Wu, S. Wang, Q. Liao, Y. Zhang, Z. L. Wang, *Adv. Funct. Mater.* **2014**, *24*, 7488.
[128] M. Chen, X. Li, L. Lin, W. Du, X. Han, J. Zhu, C. Pan, Z. L. Wang, *Adv. Funct. Mater.* **2014**, *24*, 5059.
[129] L. Jin, J. Tao, R. Bao, L. Sun, C. Pan, *Sci. Rep.* **2017**, *7*, 10521.